WALL-CAVITY AEROACOUSTICS AT LOW MACH NUMBER

M. S. Howe
Boston University, College of Engineering
110 Cummington Street, Boston MA 02215

Report No. AM-04-001
3 January, 2004

Final Report
Prepared for Dr. L. Patrick Purtell
Office of Naval Research, Code 333
Grant N00014-02-1-0549

CONTENTS

Preface

This report documents analytical studies performed to clarify the mechanisms by which sound is generated by nominally steady flow over a rectangular wall cavity. Chapter 1 (Mechanism of sound generation by low mach number flow over a wall cavity) has been accepted for publication in the *Journal of Sound and Vibration.* Chapter 2 (Wall-cavity acoustic green's function at low mach number) has been published in the *International Journal of Aeroacoustics* **2**, 347 - 365, (2003). Chapter 3 (Cavity mode excitation by vortex shedding from a cross-beam) has been written with the assistance of Ms Alia Winslow and has been submitted for publication under joint authorship in the *International Journal of Aeroacoustics.*

CHAPTER 1

MECHANISM OF SOUND GENERATION BY LOW MACH NUMBER FLOW OVER A WALL CAVITY

SUMMARY

An analysis is made of the mechanism of sound production by nominally steady low Mach number flow over a rigid shallow wall cavity. At very low Mach numbers the dominant source of sound is the unsteady drag, and the aeroacoustic dipole source accompanying this force. A monopole source dependent on the compression of fluid within the cavity is smaller by a factor of the order of the flow Mach number M. The directivity of the dipole sound peaks in directions upstream and downstream of the cavity, and there is a radiation null in the direction normal to the plane of the wall. However, numerical simulations for M as small as 0.1 have predicted significant radiation in directions normal to the wall. This anomaly is investigated in this chapter by means of an acoustic Green's function tailored to cavity geometry that accounts for possible aeroacoustic contributions from both the drag-dipole and from the lowest order cavity resonance. The Green's function is used to show that these sources are correlated and that their strengths are each proportional to the unsteady drag generated by vorticity interacting with the cavity trailing edge. When $M \sim 0.01$, the case in most underwater applications, the monopole strength is always negligible (for a cavity with rigid walls). At low Mach numbers exceeding about 0.05 it is shown that the cavity monopole radiation is $O(M^2) \ll 1$ relative to the dipole at low frequencies. At higher frequencies, near the resonance frequency of the cavity, the monopole and dipole have similar orders of magnitude, and the combination produces a relatively uniform radiation directivity, with substantial energy radiated in directions normal to the wall. Illustrative numerical results are given for a wall cavity subject to 'shear layer mode' excitation by the Rossiter 'feedback' mechanism.

1. INTRODUCTION

Tonal radiation produced by high Reynolds number mean flow over a rectangular wall cavity was originally attributed to broadband excitation of cavity acoustic resonances by turbulence in the shear layer over the cavity mouth [1]. However, oscillations can also be maintained by a laminar mean flow, and laminar flow resonances are often observed to be more intense [2, 3]. Tones generated by shallow cavities whose depth $d < L$ = streamwise cavity length (Figure 1) generally bear little or no correspondence to cavity modes and are not usually harmonically related, but are more closely analogous to the 'edge' tones excited when a thin jet impinges on a wedge-shaped knife edge, and maintained via a 'feedback' mechanism from the wedge to the jet nozzle.

A cavity tone of frequency f generated by flow of mean stream velocity U is typically found to lie within certain well defined bands of the Strouhal numbers fL/U when plotted against flow Mach number. This is consistent with the 'feedback' scheme proposed by Rossiter [1], involving the periodic formation of discrete vortices just downstream of the leading edge of the cavity, and their subsequent interaction with the trailing edge after convection across the cavity mouth. The impulsive sound generated by this interaction propagates upstream within the cavity and causes the boundary layer to separate just upstream of the leading edge. The travel time of a vortex across the cavity $\sim L/U_c$, where the convection velocity $U_c \approx 0.4U$ - $0.6U$, and the sound radiates back to the leading edge in time L/c_o, where c_o is the speed of sound. The returning sound therefore arrives in time to reinforce periodic shedding provided f satisfies [1]

$$\frac{L}{U_c} + \frac{L}{c_o} \approx \frac{n}{f}, \quad n = 1,\ 2,\ \ldots\ . \tag{1.1}$$

This formula must be adjusted to obtain detailed agreement with experiment [4 - 6], by replacing n by $n - \beta$, where β (~ 0.25) determines a 'phase lag' β/f equal to the time delay between (i) the arrival of a vortex at the trailing edge and the emission of the main acoustic pulse, and (ii) the arrival of the sound at the leading edge and the release of new vorticity. If account is also taken of the Mach number (i.e. temperature) dependence of the sound speed in the cavity, Rossiter's equation (1.1) can be written

$$\frac{fL}{U} = \frac{n - \beta}{\left\{\frac{U}{U_c} + \frac{M}{\sqrt{1+(\gamma_o - 1)M^2/2}}\right\}}, \quad n = 1,\ 2,\ \ldots\ . \tag{1.2}$$

where $M = U/c_o$ and γ_o is the ratio of specific heats of the fluid.

Predictions of the feedback formula (1.2) for shallow, rectangular cavities with $d/L < 1$ agree well with observations at $M > 0.2$ for $\beta \approx \frac{1}{4}$ and $U_c/U \approx 0.6$ [6]. The contributions from cavity resonances are important only for deep cavities, and appear to be unimportant unless $d/L > \frac{2}{5}$, when resonances can dominate the radiation provided the Strouhal number also satisfies (1.2). An extensive discussion of experimental results relating to this and other influences of cavity geometry and mean flow conditions on cavity resonances is given by Ahuja and Mendoza [6] for Mach numbers $M > 0.2$. Research prior to 1980 is reviewed by Rockwell [4] and by Rockwell & Naudascher [7], and Grace [8] has summarized recent attempts to simulate numerically cavity noise radiation.

Experiments conducted by Gharib and Roshko [9] in water with a nominally steady impinging mean flow (at $U \sim 1\,\mathrm{m/s}$) have shown that Rossiter feedback resonances are related to large fluctuations in the drag experienced by the cavity. They identified two hydrodynamic modes of cavity flow oscillations: for 'shorter' cavities relative to the upstream boundary layer thickness (and, according to later work [10], for lower Mach numbers) the unsteady motion over the cavity mouth has the characteristics of an unstable, thin shear layer ('shear layer mode') that generates sound by impingement on the cavity trailing edge, essentially in the manner proposed by Rossiter [1]. Recent numerical studies of two-dimensional cavity flows by Colonius *et al.* [10] predict strong radiation preferentially in the upstream direction, from a 'source' centred on the cavity trailing edge. Three-dimensional numerical simulations performed by Fuglsang and Cain [11] of the acoustic field *within* a shallow cavity ($L/d = 4.5$) at $M = 0.85$ also indicated that shear layer instability is the main exciting mechanism, and that it produces a source-like periodic addition and removal of mass near the trailing edge. An analytical, but empirical representation of this edge source had been previously considered by Tam and Block [12]. Flow over longer cavities (or, alternatively, at higher Mach numbers) is characterized by a 'wake mode', involving large scale vorticity ejection from the cavity, producing quasi-periodic separation upstream of the leading edge. The onset of the wake mode is accompanied by a large increase in drag fluctuations. This apparently occurs also at much higher Mach numbers. For example, numerical simulations by Zhang [13] for $L/d = 3$ and $M = 1.5,\ 3$ reveal that the violent ejection of vorticity is strongly correlated with sign reversals of the cavity drag coefficient.

The results of the shear layer mode theory of Tam and Block [12] suggested that at very low Mach numbers ($M < 0.2$) cavity acoustic resonances must contribute to the

radiation, especially for deeper cavities ($L/d < \frac{1}{2}$, say); the 'monopole' nature of such resonances would account for a near omni-directional character of the radiation pattern observed at certain frequencies. They did not pursue this theoretically, although its likely importance had already been anticipated by Plumblee *et al.* [14] and by East [15]. Similarly, experiments of Yu [16] have confirmed that shallow wall cavities in air at Mach numbers $M \sim 0.1$ radiate a substantial amount of radiation directly away from the wall. Numerical and experimental studies at low Mach number by Inagaki *et al.* [17] have confirmed this conclusion for large cavities with small openings to the mean flow, but shown also how coincidence between the cavity resonance and the Rossiter frequency predicted by (1.2) resulted in very large amplitude radiation. For shallow cavities trailing edge 'scattering' of shear layer pressure fluctuations appears to be the dominant source, even when feedback is not important. This is in accord with measurements performed by Jacobs *et al.* [18] for $L/d > 7$ and $M < 0.4$, for which the radiation peaked in the upstream and downstream directions, although significant radiation in the wall-normal direction was also observed.

According to the theoretical results of Howe [2], the radiation from a shallow cavity at very low Mach number can be ascribed to a dipole source aligned with the mean flow direction whose strength is determined by the unsteady drag. The dipole source strength is strongly coupled to the hydrodynamic motions in and near the cavity, but is essentially the same in character for both the 'shear layer' and 'wake' modes of the cavity oscillations, provided M is sufficiently small. The intensity of the dipole radiation peaks in the upstream and downstream directions, and is null in directions normal to the wall.

This conclusion is apparently incompatible with several of the experiments discussed above and with recent numerical simulations and observations at low Mach numbers. In Hardin and Pope's [19, 20] low Mach number scheme, an incompressible representation of the cavity flow is first simulated numerically, and the results are then used to evaluate acoustic 'sources' in a modified system of compressible flow equations. At $M = 0.1$ their predictions yield radiation directivities that peak in the upstream direction, but also exhibit substantial levels in directions normal to the wall, consistent with the presence of a cavity monopole field. Although various details of the approach in [19, 20] have been criticized and subjected to modification, for example by Ekaterinaris [21] and by Shen and Sorensen [22], the general characteristics of the predicted radiation are probably correct in an overall sense, if not in detail. Indeed, they accord with later numerical studies (also based on an initial determination of an incompressible approximation of the cavity flow) by Grace *et al.*

[23] and by Curtis Granda [24], that similarly predict large amplitude radiation normal to the wall.

The purpose of the present chapter is to resolve these apparent inconsistencies between numerical and analytical predictions at low Mach numbers. It will be shown that the low Mach number dipole radiation, peaking in directions upstream and downstream of the cavity, is indeed the dominant source at very low Mach numbers, typically much smaller than $M = 0.1$, however. Thus, it is this source that determines cavity radiation in underwater applications (where $M \sim 0.01$) provided, of course, that the cavity walls are sufficiently 'rigid' to preclude monopole sources produced by pulsations in the cavity volume. But, when $M \sim 0.1$ we shall show that the cavity 'Helmholtz' mode, although very weak and formally vanishingly small as $fL/U \to 0$, supplies an additional, omni-directional contribution that can exceed the drag dipole radiation over a range of frequencies. Furthermore, it will be shown that the monopole and dipole source strengths are *both* determined at low Mach numbers by the cavity drag fluctuations.

The low Mach number analysis will be framed in terms of the theory of vortex sound [3], and the relevant equations are recalled in §2. The possible source types are identified by introducing an acoustic Green's function that is valid in the presence of low Mach number mean stream flow past the cavity (§3). At very low Mach numbers the acoustic amplitudes are always small enough for incompressible flow to be regarded as an excellent first approximation to the motion in the cavity. This flow determines the effective vortex sound source strengths, irrespective of whether the flow is characterized as 'shear layer' or 'wake' mode. Predictions of the theory are therefore illustrated in §4 for the simpler case of shear mode flow by means of an idealized model of shear layer excitation.

2. FORMULATION

Consider nominally steady, low Mach number, high Reynolds number mean flow in the positive x_1-direction of the rectangular coordinates (x_1, x_2, x_3) over the rectangular wall cavity of Figure 1. The wall and the interior surfaces of the cavity are assumed to be rigid. The fluid has mean density and sound speed respectively equal to ρ_o, c_o, and the velocity in the main stream is U. The cavity has depth d and breadth b, and is aligned with its remaining side of length L parallel to the mean flow. The coordinate origin is taken at O in the plane of the wall at the centre of the cavity mouth, with the x_2-axis normal to the wall and directed into the main stream.

Sound is produced by flow instability in the neighbourhood of the cavity. According to Lighthill's acoustic analogy [3], when the total enthalpy B, say, is taken as the acoustic variable, the radiation can be expressed in terms of sources that represent excitation by vorticity and entropy fluctuations. For a nominally homogeneous flow at low Mach numbers the motion may be regarded as homentropic to a good approximation [25]. In that case the total enthalpy becomes

$$B = \int \frac{dp}{\rho} + \frac{1}{2}v^2, \tag{2.1}$$

where ρ is fluid density, $p \equiv p(\rho)$ the pressure, and $\mathbf{v}$ denotes velocity, and Lighthill's acoustic analogy equation becomes

$$\left(\frac{D}{Dt}\left(\frac{1}{c^2}\frac{D}{Dt}\right) - \frac{1}{\rho}\nabla\cdot(\rho\nabla)\right) B = \frac{1}{\rho}\mathrm{div}(\rho\boldsymbol{\omega}\wedge\mathbf{v}), \tag{2.2}$$

where c is the local speed of sound. In the irrotational acoustic far field Crocco's form of the momentum equation $\partial\mathbf{v}/\partial t = -\nabla B$ implies that $B = -\partial\varphi/\partial t$, where $\varphi(\mathbf{x}, t)$ is the velocity potential that determines the whole motion in the irrotational regions of the fluid. B is therefore equal to a *constant* in a steady mean flow, and at large distances from the sources perturbations in B represent outgoing sound waves.

In the particular case of low Mach number flow, when $M = U/c_o$ is smaller than about 0.2, say, so that $M^2 \ll 1$, the characteristics of the motion within and close to the cavity will be essentially the same as if the fluid is incompressible, the acoustic component constituting a very small perturbation about this motion. We can then replace ρ and c where they occur explicitly in (2.2) by their respective mean values ρ_o and c_o. On the left hand side we can also introduce the approximation (valid to first order in M)

$$\frac{1}{c_o^2}\frac{D^2}{Dt^2} \approx \frac{1}{c_o^2}\frac{\partial^2}{\partial t^2} + \frac{2}{c_o^2}\mathbf{U_o}\cdot\nabla\frac{\partial}{\partial t}$$

where $\mathbf{U_o} \equiv \mathbf{U_o}(\mathbf{x})$ is the undisturbed local mean velocity, which satisfies $\mathbf{U_o} \to (U, 0, 0)$ as $|\mathbf{x}| \to \infty$.

Equation (2.2) accordingly reduces to

$$\left\{\frac{1}{c_o^2}\left(\frac{\partial^2}{\partial t^2} + 2\mathbf{U_o}\cdot\nabla\frac{\partial}{\partial t}\right) - \nabla^2\right\} B = \mathrm{div}(\boldsymbol{\omega}\wedge\mathbf{v}). \tag{2.3}$$

At large distances from the cavity fluctuations in $B \equiv B(\mathbf{x}, t)$ represent outgoing sound waves generated by the vortex source on the right of (2.3) and by its interactions with the cavity. B may therefore be assumed to vanish in the absence of radiation from the cavity, in which case if $p(\mathbf{x}, t)$ now represents the perturbation pressure, it is readily deduced from (2.1) that in the acoustic far field ([3], page 161)

$$p = \frac{\rho_o B}{(1 + M\cos\theta)}, \quad |\mathbf{x}| \to \infty, \quad \text{where} \quad \cos\theta = \frac{x_1}{|\mathbf{x}|}. \tag{2.4}$$

3. SOLUTION OF THE AERODYNAMIC SOUND EQUATION

3.1 Green's function

The steady mean velocity $\mathbf{U}_o(\mathbf{x})$ must be irrotational in the absence of sound production at the cavity. When $M^2 \ll 1$ it may be assumed to represent an incompressible flow whose details near the cavity depend on cavity geometry. To define this flow we introduce the Kirchhoff vector $\mathbf{X}(\mathbf{x}) = (X_1(\mathbf{x}), 0, X_3(\mathbf{x}))$ for the cavity, where X_j $(j = 1, 3)$ is the solution of following potential flow problem

$$\nabla^2 X_j = 0, \quad X_j \to x_j \ \text{ as } |\mathbf{x}| \to \infty, \ \ \frac{\partial X_j}{\partial x_n} = 0 \text{ on S}, \tag{3.1}$$

where S is the rigid boundary consisting of the wall and cavity surfaces, and x_n is distance measured in the normal direction from S. $X_j(\mathbf{x})$ $(j = 1, 3)$ is just the velocity potential of flow over the cavity in the j-direction that has unit speed in the j-direction at large distances from the cavity.

Then the mean flow velocity $\mathbf{U}_o = U\nabla X_1(\mathbf{x})$, which can also be written

$$\mathbf{U}_o = \nabla\{\mathbf{U}\cdot\mathbf{X}(\mathbf{x})\}, \quad \text{where } \ \mathbf{U} = (U, 0, 0). \tag{3.2}$$

To determine the solution of the aerodynamic sound equation (2.3) when $\mathbf{U}_o$ is defined in this way we consider first the Green's function $G(\mathbf{x}, \mathbf{y}, t-\tau)$, which is the solution with outgoing wave behaviour when the right hand side of (2.3) is replaced by the point source $\delta(\mathbf{x}-\mathbf{y})\delta(t-\tau)$. Because $B = -\partial\varphi/\partial t$ for irrotational motions, Green's function G is required to have vanishing normal derivative on S. Introduce the transformation [3, 26]

$$G(\mathbf{x}, \mathbf{y}, t-\tau) = -\frac{1}{2\pi}\int_{-\infty}^{\infty} \hat{G}(\mathbf{x}, \mathbf{y}, \omega) \mathrm{e}^{-i\omega(t-\tau+\mathbf{M}\cdot(\mathbf{X}-\mathbf{Y})/c_o)} d\omega, \tag{3.3}$$

where $\mathbf{M} = \mathbf{U}/c_o$, and $\mathbf{Y} = (Y_1, 0, Y_3)$ is the Kirchhoff vector expressed in terms of $\mathbf{y}$, then when $M^2 \ll 1$, $\hat{G}$ satisfies

$$\left(\nabla^2 + \kappa_o^2\right)\hat{G} = \delta(\mathbf{x}-\mathbf{y}), \quad \frac{\partial \hat{G}}{\partial x_n} = 0 \text{ on S}, \tag{3.4}$$

where $\kappa_o = \omega/c_o$ is the acoustic wavenumber.

In the cavity radiation problem the source point $\mathbf{y}$ is within or near the cavity, and the observation point $\mathbf{x}$ is in the main stream, at large distances from the cavity. In these circumstances an analytical approximation to the solution of (3.4) can be derived by a

familiar procedure [3] that involves a straightforward application of the reciprocal theorem $\hat{G}(\mathbf{x},\mathbf{y},\omega) = \hat{G}(\mathbf{y},\mathbf{x},\omega)$ [27]: the roles of $\mathbf{x}$ and $\mathbf{y}$ are interchanged in (3.4), which is now to be solved *as a function of* $\mathbf{y}$ for the reciprocal configuration in which the source is placed at the far field point $\mathbf{x}$. The distant source generates a spherical wave that may be regarded as locally plane when it arrives at the wall cavity. This greatly simplifies the problem when the characteristic wavelength $\sim 2\pi/\kappa_o$ of the sound is large compared to the typical cavity dimension, which is the case at sufficiently small Mach numbers. We can then anticipate that there are two principal contributions to the cavity response to the impinging wave: a monopole component produced by a periodic volume flux across the plane of the cavity mouth, corresponding to 'breathing' oscillations in the manner of a Helmholtz resonator [27], and a dipole field, with dipole axis parallel to the plane of the wall, representing an unsteady drag force on the cavity.

Therefore, in the usual way [3] for $\mathbf{y}$ within and near the cavity and $|\mathbf{x}| \to \infty$, we put

$$\hat{G} \approx \hat{G}_0 + \hat{G}_{\mathrm{M}} + \hat{G}_{\mathrm{D}}, \tag{3.5}$$

where $\hat{G}_0$ represents the uniform pressure produced by the incident wave in the neighbourhood of the cavity, and $\hat{G}_{\mathrm{M}}$ and $\hat{G}_{\mathrm{D}}$ respectively represent the monopole and dipole fields near the cavity.

In the absence of the cavity the exact Green's function is

$$\hat{G} = -\frac{\mathrm{e}^{i\kappa_o|\mathbf{x}-\mathbf{y}|}}{4\pi|\mathbf{x}-\mathbf{y}|} - \frac{\mathrm{e}^{i\kappa_o|\bar{\mathbf{x}}-\mathbf{y}|}}{4\pi|\bar{\mathbf{x}}-\mathbf{y}|}, \quad \bar{\mathbf{x}} = (x_1, -x_2, x_3), \tag{3.6}$$

which satisfies $\partial\hat{G}/\partial y_2 = 0$ on the plane surface $y_2 = 0$ of the wall. When $\kappa_o|\mathbf{y}| \ll 1$ and $\kappa_o|\mathbf{x}| \gg 1$ this becomes

$$\hat{G} \approx -\frac{\mathrm{e}^{i\kappa_o|\mathbf{x}|}}{2\pi|\mathbf{x}|} + \frac{i\kappa_o(\mathbf{x}+\bar{\mathbf{x}})\cdot\mathbf{y}\,\mathrm{e}^{i\kappa_o|\mathbf{x}|}}{4\pi|\mathbf{x}|^2} + \cdots \tag{3.7}$$

where the terms omitted are of order $\sim (\kappa_o|\mathbf{y}|)^2$ and smaller. The first term on the right hand side represents (as a function of $\mathbf{y}$) a uniform pressure fluctuation over the mouth of the cavity and must therefore correspond to $\hat{G}_0$. The second term $\sim \mathrm{O}(\kappa_o|\mathbf{y}|)$, and satisfies as a function of $\mathbf{y}$ Laplace's equation to this order. It is the velocity potential of a uniform, incompressible flow parallel to the wall (because $\mathbf{x}+\bar{\mathbf{x}} = 2(x_1, 0, x_3)$), and must be augmented by a suitable solution of Laplace's equation that accounts for the presence of the cavity (and in particular for the singular behaviour of $\hat{G}$ near the cavity edges) and

describes the diversion of this flow into and out of the cavity mouth. The definition (3.1) of the Kirchhoff vector enables this to be accomplished simply by replacing $(\mathbf{x}+\bar{\mathbf{x}})\cdot\mathbf{y}$ by $(\mathbf{x}+\bar{\mathbf{x}})\cdot\mathbf{Y}\equiv 2\mathbf{x}\cdot\mathbf{Y}$.

Thus,

$$\hat{G}_0=-\frac{\mathrm{e}^{i\kappa_o|\mathbf{x}|}}{2\pi|\mathbf{x}|},\qquad \hat{G}_{\mathrm{D}}=\frac{i\kappa_o\mathbf{x}\cdot\mathbf{Y}\,\mathrm{e}^{i\kappa_o|\mathbf{x}|}}{2\pi|\mathbf{x}|^2}, \tag{3.8}$$

and it remains to determine $\hat{G}_{\mathrm{M}}$.

The uniform incident applied pressure distribution $\hat{G}_0$ over the mouth of a cavity of depth d produces vertically orientated compressional motions described by the following representations:

$$\hat{G} \;=\; \alpha\cos\{\kappa_o(y_2+d)\},\quad \text{within the cavity in}\quad -d<y_2<0, \tag{3.9}$$

$$\left.\begin{aligned}\hat{G}_{\mathrm{M}} \;&=\; \beta\varphi^*(\mathbf{y})+\gamma,\quad \text{in the cavity mouth}\quad y_2\sim 0,\\ &=\; -\frac{\delta\mathcal{A}}{2\pi|\mathbf{y}|}\,\mathrm{e}^{i\kappa_o|\mathbf{y}|},\quad \text{in free space above the cavity}\quad y_2\gg L,\end{aligned}\right\} \tag{3.10}$$

where α, β, γ, δ are constant coefficients, $\mathcal{A}=bL$ is the area of the cavity mouth, and $\varphi^*(\mathbf{y})$ is the solution of Laplace's equation describing uniform flow from the mouth, normalized such that

$$\varphi^*(\mathbf{y}) \;\sim\; -\frac{\mathcal{A}}{2\pi|\mathbf{y}|}\quad |\mathbf{y}|\gg d,\ \text{above the cavity} \tag{3.11}$$

$$\sim\; y_2-\ell,\quad y_2\to -d\ \text{within the cavity}, \tag{3.12}$$

$\ell\sim\sqrt{\pi\mathcal{A}}/4$ is the 'end correction' of the mouth [3, 27].

Equations determining the values of the coefficients α, β, γ, δ are obtained by matching the various representations of $\hat{G}$ and $\hat{G}_{\mathrm{M}}$. Thus, in the region $\kappa_o|\mathbf{y}|\ll 1$ just above the cavity mouth, equations (3.10) and (3.11) imply that

$$-\frac{\beta\mathcal{A}}{2\pi|\mathbf{y}|}+\gamma\equiv-\frac{\delta\mathcal{A}}{2\pi|\mathbf{y}|}-\frac{i\delta\kappa_o\mathcal{A}}{2\pi},$$

from which it follows that $\delta=\beta$ and $\gamma=-i\beta\kappa_o\mathcal{A}/2\pi$, and therefore that

$$\hat{G}_{\mathrm{M}}=\beta\left(\varphi^*(\mathbf{y})-\frac{i\kappa_o\mathcal{A}}{2\pi}\right),\quad \text{in the cavity mouth.} \tag{3.13}$$

Similarly, within the cavity the representation (3.9) must match just below the cavity mouth with the continuation of $\hat{G} = \hat{G}_0 + \hat{G}_{\rm M} + \hat{G}_{\rm D}$ given by (3.8) and (3.13). Now $\mathbf{Y}$ must decrease exponentially fast with distance into the cavity ([28], Section 66), and therefore (using (3.9) and (3.12))

$$\alpha\cos(\kappa_o d) - \alpha\kappa_o y_2 \sin(\kappa_o d) \equiv \beta\left(y_2 - \ell - \frac{i\kappa_o \mathcal{A}}{2\pi}\right) + \hat{G}_0,$$

from which it follows, in particular, that

$$\begin{aligned}\hat{G}_{\rm M} &\approx \left(\varphi^*(\mathbf{y}) - \frac{i\kappa_o\mathcal{A}}{2\pi}\right)\frac{e^{i\kappa_o|\mathbf{x}|}}{2\pi|\mathbf{x}|}\Bigg/\left(\frac{1}{\kappa_o\tan(\kappa_o d)} - \ell - \frac{i\kappa_o\mathcal{A}}{2\pi}\right)\\ &\approx \left(\varphi^*(\mathbf{y}) - \frac{i\kappa_o\mathcal{A}}{2\pi}\right)\frac{\kappa_o\sin(\kappa_o d)}{\cos\{\kappa_o(d+\ell+i\kappa_o\mathcal{A}/2\pi)\}}\frac{e^{i\kappa_o|\mathbf{x}|}}{2\pi|\mathbf{x}|}. \qquad (3.14)\end{aligned}$$

The steps in the derivation of this approximation for $\hat{G}_{\rm M}$ are strictly valid only for a deep cavity (so that $\kappa_o\ell$, $\kappa_o^2\mathcal{A}/2\pi \ll 1$), but if necessary it may be assumed that the values of ℓ and $\mathcal{A}$ are suitably adjusted to ensure the validity of the second line of (3.14). The depth mode resonance frequencies are determined by the zeros of the cosine term in the denominator of the second line of (3.14). The lowest order mode occurs at the complex frequency satisfying

$$\kappa_o\left(d + \ell + \frac{i\kappa_o\mathcal{A}}{2\pi}\right) = \frac{\pi}{2},$$

that is for

$$\kappa_o d \sim \frac{\pi d}{2(d+\ell)} - \frac{i\pi\mathcal{A}d}{8(d+\ell)^3}. \qquad (3.15)$$

The real part is the usual expression for the lowest order depth mode for a cavity whose depth d is augmented by the end correction ℓ, which represents the effective length by which the cavity must be extended to account for the inertia of fluid above the mouth of the cavity also set into reciprocating motion by the cavity resonance; the imaginary part accounts for the damping of this mode by radiation into the fluid.

Tam [29] has shown for the case of *two-dimensional* rectangular cavities that the frequency of the lowest order mode is well represented by (3.15) even for d/L as small as 1, for a suitable choice of the value of ℓ. For deep cavities we can use Rayleigh's [27] approximation

$$\ell \sim \frac{\sqrt{\pi\mathcal{A}}}{4}. \qquad (3.16)$$

For the purpose of the numerical illustrations given below for the moderately shallow case of $d/L = 0.5$ it will be sufficient to use (3.16) – in practice precise values of ℓ can always be derived from a numerical simulation of the acoustic mode.

The complex factor in the argument of the cosine term in (3.14) increases rapidly with κ_o, showing that higher order modes of the cavity are strongly damped by radiation losses. Thus, we can anticipate that only the lowest order 'Helmholtz resonator' mode (3.15) of the cavity will be of any importance in applications to cavity flow-noise, although this is not persued further here.

Hence, substituting (3.8) and (3.14) in (3.5), and using the inversion formula (3.3), it follows that for $\mathbf{y}$ in the neighbourhood of the cavity mouth and $\mathbf{x}$ in the acoustic far field,

$$\begin{aligned} G(\mathbf{x},\mathbf{y},t-\tau) &\approx -\frac{1}{2\pi}\int_{-\infty}^{\infty}\left(\hat{G}_0+\hat{G}_{\rm M}+\hat{G}_{\rm D}\right)(\mathbf{x},\mathbf{y},\omega)\mathrm{e}^{-i\omega(t-\tau+\mathbf{M}\cdot(\mathbf{X}-\mathbf{Y})/c_o)}d\omega, \\ &= \frac{1}{(2\pi)^2|\mathbf{x}|}\int_{-\infty}^{\infty}\left\{1-\left(\varphi^*(\mathbf{y})-\frac{i\kappa_o\mathcal{A}}{2\pi}\right)\frac{\kappa_o\sin(\kappa_o d)}{\cos\{\kappa_o(d+\ell+i\kappa_o\mathcal{A}/2\pi)\}}\right. \\ &\qquad \left.-\frac{i\kappa_o\mathbf{x}\cdot\mathbf{Y}}{|\mathbf{x}|}\right\}\mathrm{e}^{-i\omega(t-\tau-|\mathbf{x}|/c_o+\mathbf{M}\cdot(\mathbf{X}-\mathbf{Y})/c_o)}\,d\omega. \end{aligned} \tag{3.17}$$

To interpret this result, observe first that cavity resonance corresponds to $\kappa_o d \sim O(1)$. At such frequencies the second term in the brace brackets of the integrand, involving $\mathbf{Y}$, is not important. The latter is becomes significant away from resonances, and then only when the source point $\mathbf{y}$ is close to a cavity edge. The basic assumption is that very high frequencies (in excess of the first cavity resonance) are irrelevant, and this will be the case when excitation occurs at low Mach numbers.

3.2 The radiated sound

The Green's function (3.17) now permits the solution of the aerodynamic sound equation (2.3), where B is given by (2.4) in the far field, to be expressed in the form [3]

$$p \approx \frac{-\rho_o}{(1+M\cos\theta)}\int(\boldsymbol{\omega}\wedge\mathbf{v})(\mathbf{y},\tau)\cdot\frac{\partial G}{\partial\mathbf{y}}(\mathbf{x},\mathbf{y},t-\tau)\,d^3\mathbf{y}d\tau, \quad |\mathbf{x}|\to\infty, \tag{3.18}$$

where the integration is over all values of the retarded time τ and the fluid region where the vorticity $\boldsymbol{\omega}\neq\mathbf{0}$. There are no contributions from surface integrals over the wall and

cavity, on which the fluid normal component of velocity and the normal derivative of G both vanish.

It follows from this result that only the $\mathbf{y}$-dependent part of the Green's function (3.17) need be used in (3.18). Therefore, for small Mach numbers and an acoustically compact source flow, the acoustic pressure given by (3.18) can be reduced to the form

$$p \approx \frac{\rho_o}{(2\pi)^2(1+M\cos\theta)|\mathbf{x}|}\int(\boldsymbol{\omega}\wedge\mathbf{v})(\mathbf{y},\tau)\cdot\frac{\partial}{\partial\mathbf{y}}\int_{-\infty}^{\infty}\left\{\frac{\varphi^*(\mathbf{y})\kappa_o\sin(\kappa_o d)}{\cos\{\kappa_o(d+\ell+i\kappa_o\mathcal{A}/2\pi)\}}\right.$$

$$\left.+\,i\kappa_o\left(\frac{\mathbf{x}}{|\mathbf{x}|}-\mathbf{M}\right)\cdot\mathbf{Y}\right\}e^{-i\omega\{t-\tau-(|\mathbf{x}|-\mathbf{M}\cdot\mathbf{x})/c_o\}}\,d\omega d^3\mathbf{y}d\tau,\quad|\mathbf{x}|\to\infty. \tag{3.19}$$

3.3 Leading edge Kutta condition

In a typical oscillatory cavity flow the region within, above and downstream of the cavity is filled with vorticity generated by shedding, principally from the leading edge region of the cavity. The length scales of the unsteady hydrodynamic motions induced by this vorticity are comparable to the cavity length L, but the characteristic extent of a coherent region of vorticity is usually very much smaller. This means that the main contributions to the volume integral in (3.19) are from those regions where $\nabla\varphi^*$ and ∇Y_j ($j = 1,\ 3$) vary rapidly, since $\int(\boldsymbol{\omega}\wedge\mathbf{v})(\mathbf{y},\tau)\,d^3\mathbf{y}\sim\mathbf{0}$ in regions where $\nabla\varphi^*$ and ∇Y_j can be regarded as constant or as varying very slowly relative to the length scale of the vorticity.

It follows that the cavity *edges* at which $\nabla\varphi^*$ and ∇Y_j become infinite are the main sources of the cavity radiation, and a good estimate of the value of the integral can therefore be obtained by expanding these derivatives about these edges. In doing this we can explicitly discard any contributions from the *leading edge* of the cavity, because the Kutta condition ensures that acoustic excitation by cavity vorticity interacting with this edge is inhibited by the shedding of fresh vorticity [2, 3, 30 - 32]. Similarly, the contributions from the side edges of the cavity (parallel to the mean flow direction) are small, because the vortex source $\boldsymbol{\omega}\wedge\mathbf{v}$ convects predominantly in the mean flow direction so that its interaction with the edge is effectively invariant with time (i.e. it is 'silent'). We therefore conclude, in accordance with all previous observations, that it is primarily the trailing edge of the cavity that is responsible for the radiated sound.

Recall that Y_j ($j = 1,\ 3$) may be interpreted as the velocity potential of a uniform flow over the cavity in the j-direction. This means that $|\nabla Y_3| \ll |\nabla Y_1|$ at the cavity trailing

edge, and therefore that the contribution from Y_3 in (3.19) can be discarded. If we now introduce a 'strip theory' approximation for Y_1 in the immediate vicinity of the edge, by equating it to the corresponding velocity potential for flow over a two-dimensional cavity, which is readily found by conformal mapping, we find (for details see [3])

$$Y_1(\mathbf{y}) \sim C_1 L^{\frac{1}{3}} \mathrm{Re}\left(z^{\frac{2}{3}}\right), \quad \text{where} \quad z = y_1 - \frac{L}{2} + iy_2 \quad \text{and} \quad C_1 = \frac{3}{2}\left[\frac{(1-\mu)}{6\mathrm{E}(\mu)}\right]^{\frac{1}{3}}, \tag{3.20}$$

where μ is the solution of the equation

$$\frac{\mathrm{K}(1-\mu) - \mathrm{E}(1-\mu)}{\mathrm{E}(\mu)} = \frac{d}{L} \tag{3.21}$$

and $\mathrm{K}(\xi) = \int_0^{\frac{\pi}{2}} d\lambda/\sqrt{1-\xi\sin^2\lambda}$, $\mathrm{E}(\xi) = \int_0^{\frac{\pi}{2}} \sqrt{1-\xi\sin^2\lambda}\, d\lambda$ $(0 < \xi < 1)$ are complete elliptic integrals [33].

A similar strip-theory calculation reveals that near the trailing edge

$$\varphi^*(\mathbf{y}) \sim C_2 Y_1(\mathbf{y}), \quad C_2 = 2\left[\frac{\mathrm{E}(\mu)}{4\pi(1-\mu)}\right]^{\frac{1}{3}}. \tag{3.22}$$

Hence, (3.19) becomes

$$\begin{aligned} p \;\approx\; & \frac{\rho_o}{(2\pi)^2(1+M\cos\theta)|\mathbf{x}|}\int (\boldsymbol{\omega}\wedge\mathbf{v})(\mathbf{y},\tau)\cdot\frac{\partial Y_1}{\partial \mathbf{y}}(\mathbf{y})\, d^3\mathbf{y} \\ & \times \int_{-\infty}^{\infty} \kappa_o \left(\frac{C_2\sin(\kappa_o d)}{\cos\{\kappa_o(d+\ell+i\kappa_o\mathcal{A}/2\pi)\}} + i\,(\cos\theta - M)\right) \mathrm{e}^{-i\omega\{t-\tau-(|\mathbf{x}|-\mathbf{M}\cdot\mathbf{x})/c_o\}}\, d\omega d\tau, \\ & \qquad\qquad |\mathbf{x}| \to \infty, \end{aligned} \tag{3.23}$$

where Y_1 is given by (3.20).

3.4 Physical interpretation

The first and second terms in the large brackets of (3.23) correspond respectively to monopole and dipole radiation from the cavity. The monopole character of the first term should be obvious from the discussion in §3.1. To understand the dipole nature of the second term note first that equation (3.23) is the acoustic pressure as measured by an observer *fixed relative to the cavity*, and therefore moving at speed U in the negative x_1-direction relative

to the mean stream. Let $\mathbf{R}$ be the vector position relative to the cavity of an observer in a reference frame moving with the fluid *at the time of emission* of the arriving sound. For such an observer the cavity appears to translate at speed U in the negative x_1-direction. The coordinate systems $\mathbf{x}$ and $\mathbf{R}$ are related by (see Figure 2) $\mathbf{x} = \mathbf{R} + \mathbf{M}R$, since an observer fixed relative to the fluid moves a distance $U \times (R/c_o)$ in the x_1-direction relative to the cavity during the time of travel R/c_o of the sound from the cavity to the observer. The following relations are now easily derived for small M:

$$|\mathbf{x}| - \mathbf{M}\cdot\mathbf{x} = |\mathbf{R}|, \quad |\mathbf{x}| = |\mathbf{R}|(1 + M\cos\Theta), \quad \cos\theta - M = \frac{\cos\Theta}{(1 + M\cos\Theta)}, \tag{3.24}$$

where Θ is the angle between the observer direction and the mean flow direction at the time of emission of the sound.

Making these substitutions in (3.23) we find, for small M,

$$\begin{aligned} p \;\approx\; & \frac{\rho_o}{(2\pi)^2(1 + M\cos\Theta)^2|\mathbf{R}|}\int(\boldsymbol{\omega}\wedge\mathbf{v})(\mathbf{y},\tau)\cdot\frac{\partial Y_1}{\partial\mathbf{y}}(\mathbf{y})\,d^3\mathbf{y} \\ & \times\int_{-\infty}^{\infty}\kappa_o\left(\frac{C_2\sin(\kappa_o d)}{\cos\{\kappa_o(d+\ell+i\kappa_o\mathcal{A}/2\pi)\}} + \frac{i\cos\Theta}{(1+M\cos\Theta)}\right)\mathrm{e}^{-i\omega\{t-\tau-|\mathbf{R}|/c_o\}}\,d\omega d\tau, \\ & \qquad\qquad |\mathbf{R}|\to\infty, \end{aligned} \tag{3.25}$$

where Y_1 is given by (3.20). This formula represents the radiation measured by a fixed observer from a uniformly translating cavity as being equal to the sum of a monopole amplified by the familiar two powers of the Döppler factor $1/(1 + M\cos\Theta)$ together with a surface interaction dipole magnified by three Döppler factors (c.f. Crighton [34]).

The strengths of the monopole and dipole sources are both determined by the value of the integral

$$F(\tau) = \rho_o\int(\boldsymbol{\omega}\wedge\mathbf{v})(\mathbf{y},\tau)\cdot\frac{\partial Y_1}{\partial\mathbf{y}}(\mathbf{y})\,d^3\mathbf{y}, \tag{3.26}$$

which is just the force exerted on the cavity in the x_1-direction (i.e. the cavity *drag*) when the unsteady flow in the vicinity of the cavity is regarded as incompressible [3]. Only the *unsteady* component of the drag actually contributes to the radiation, and it may therefore be assumed that the mean component of the drag has been excluded, and that henceforth $F(t)$ refers only to the fluctuating part, having zero mean value. Then, for example,

equation (3.23) becomes

$$p \approx \frac{1}{2\pi(1+M\cos\theta)|\mathbf{x}|}\int_{-\infty}^{\infty}\hat{F}(\omega)\,\kappa_o\left(\frac{C_2\sin(\kappa_o d)}{\cos\{\kappa_o(d+\ell+i\kappa_o\mathcal{A}/2\pi)\}}+\,i\,(\cos\theta-M)\right)$$

$$\times\, \mathrm{e}^{-i\omega\{t-(|\mathbf{x}|-\mathbf{M}\cdot\mathbf{x})/c_o\}}\,d\omega, \quad |\mathbf{x}|\to\infty, \tag{3.27}$$

where

$$\hat{F}(\omega)=\frac{1}{2\pi}\int_{-\infty}^{\infty}F(t)\mathrm{e}^{i\omega t}\,dt \tag{3.28}$$

is the Fourier transform of the fluctuating drag.

4. NUMERICAL ILLUSTRATION

4.1 Acoustic pressure frequency spectrum

The unsteady drag $F(t)$ may be assumed to be a stationary random function of the time, whose ('two-sided') spectrum $\Psi(\omega)$, say, satisfies

$$\langle F(\omega)F^*(\omega')\rangle = \Psi(\omega)\delta(\omega-\omega'), \tag{4.1}$$

where the angle brackets $\langle\ \rangle$ represent a time or ensemble average, and the asterisk denotes complex conjugate. For the low Mach number flows encompassed by the present theory $\Psi(\omega)$ can be found from measurement or by numerical simulation of the essentially incompressible cavity flow. When known it can be used in conjunction with (3.27) to calculate the far field acoustic pressure frequency spectrum, which will be denoted by $\Phi(\omega,\mathbf{x})$, and defined such that

$$\langle p^2(\mathbf{x},t)\rangle = \int_0^\infty \Phi(\omega,\mathbf{x})\,d\omega. \tag{4.2}$$

Thus, using (3.27) and the definition (4.1), we find

$$\Phi(\omega,\mathbf{x}) \approx \frac{\Psi(\omega)\kappa_o^2}{2\pi^2(1+M\cos\theta)^2|\mathbf{x}|^2}\left|\frac{C_2\sin(\kappa_o d)}{\cos\{\kappa_o(d+\ell+i\kappa_o\mathcal{A}/2\pi)\}} + i\,(\cos\theta - M)\right|^2, \quad |\mathbf{x}|\to\infty. \tag{4.3}$$

This formula gives the frequency dependence with respect to an observer fixed relative to the cavity. If the cavity is attached to a moving body, and the observer is at rest relative to the fluid, the observed frequency Ω will have the Döppler shifted value

$$\Omega = \frac{\omega}{1+M\cos\Theta}, \tag{4.4}$$

so that if $\langle p^2(\mathbf{R},t)\rangle = \int_0^\infty \Phi(\Omega,\mathbf{R})\,d\Omega$, then

$$\Phi(\Omega,\mathbf{R}) \approx \frac{\Psi(\omega)\kappa_o^2}{2\pi^2(1+M\cos\Theta)^3|\mathbf{R}|^2}\left|\frac{C_2\sin(\kappa_o d)}{\cos\{\kappa_o(d+\ell+i\kappa_o\mathcal{A}/2\pi)\}} + \frac{i\cos\Theta}{(1+M\cos\Theta)}\right|^2, \quad |\mathbf{R}|\to\infty, \tag{4.5}$$

in which ω and $\kappa_o = \omega/c_o$ are defined in terms of Ω as in (4.4).

4.2 Analytical model for shear layer mode radiation

To illustrate predictions of (4.3) a simple yet mathematically tractable model will now be considered for a shallow cavity subject to shear layer mode excitation. The principal

aerodynamic sources $\mathrm{div}(\boldsymbol{\omega}\wedge\mathbf{v})$ on the right of equation (2.3) are then confined to the region above the cavity mouth. In a first approximation the flow is parallel to the x_1-direction, so that the main contribution to the drag integral (3.26) (wherein Y_1 is given approximately by (3.20)) is determined by the *spanwise* component ω_3 of the vorticity.

We therefore write

$$(\boldsymbol{\omega}\wedge\mathbf{v})(\mathbf{y},\tau)\approx\mathbf{j}\int_{-\infty}^{\infty}\mathcal{F}(k,k_\perp,\omega,y_2)\mathrm{e}^{i(ky_1+k_\perp y_3-\omega\tau)}\,dkdk_\perp d\omega,\quad y_2>0,\quad |y_3|<\frac{b}{2},\tag{4.6}$$

where $\mathbf{j}$ is a unit vector in the x_2-direction, normal to the plane of the wall, and $\mathcal{F}(k,k_\perp,\omega,y_2)$ determines the distribution across the shear layer of harmonic constituents of the unsteady shear flow of frequency ω and with streamwise and spanwise wavelengths respectively equal to $2\pi/k$ and $2\pi/k_\perp$. Inserting this formula into the integral of (3.26), and using the local approximation (3.20) for Y_1, the y_1-integral is readily evaluated to yield the Fourier transform $\hat{F}(\omega)$ of the unsteady drag in the form

$$\hat{F}(\omega)=\frac{C_1\Gamma(\frac{2}{3})L^{\frac{1}{3}}}{\sqrt{3}}\rho_o\int\frac{\mathcal{F}(k,k_\perp,\omega,y_2)}{(k-i0)^{\frac{2}{3}}}\,\mathrm{e}^{i(k_\perp y_3-\frac{\pi}{3})-|k|y_2}\,dkdk_\perp dy_2dy_3,\tag{4.7}$$

where the notation '$-i0$' implies that the branch cut for $(k-i0)^{\frac{2}{3}}$ is to be taken from $k=0$ to $+i\infty$ in the upper half-plane.

This result can be cast in a more useful form in terms of the hydrodynamic pressure fluctuations p_s, say, that the same flow would exert on the rigid wall *in the absence of the cavity*. This is usually called the 'blocked surface pressure', and in a first approximation may be identified with the (measurable) wall surface pressure fluctuations just downstream of the cavity. At low Mach numbers we can regard this pressure as that generated by the shear layer vorticity when the flow is incompressible, and it is therefore determined by the incompressible form of equation (2.2)

$$\nabla^2 B=-\mathrm{div}(\boldsymbol{\omega}\wedge\mathbf{v}),\quad x_2>0,\quad\text{where}\quad p_s=\rho_o B\quad\text{on } x_2=0.\tag{4.8}$$

When $\boldsymbol{\omega}\wedge\mathbf{v}$ is given by (4.6) a routine calculation [3] yields

$$p_s=\int_{-\infty}^{\infty}\hat{p}_s(k,k_\perp,\omega)\mathrm{e}^{i(ky_1+k_\perp y_3-\omega t)}\,dkdk_\perp d\omega,\tag{4.9}$$

where

$$\hat{p}_s(k,k_\perp,\omega)=\frac{\rho_o}{2}\int_0^\infty\mathcal{F}(k,k_\perp,\omega,y_2)\mathrm{e}^{-\{k^2+k_\perp^2\}^{\frac{1}{2}}y_2}\,dy_2.\tag{4.10}$$

Now $k \sim \omega/U_c$ at those values of the wavenumber k where the blocked pressure Fourier amplitude $\hat{p}_s(k, k_\perp, \omega)$ is significant. Because the motion over the cavity can be regarded as locally two-dimensional, the corresponding typical values of the spanwise wavenumber $k_\perp \ll k$. Thus, $\{k^2 + k_\perp^2\}^{\frac{1}{2}}$ can be replaced by $|k|$ in the exponential of (4.10), and it is then deduced from (4.7) that

$$\hat{F}(\omega) \approx \frac{2C_1\Gamma(\frac{2}{3})L^{\frac{1}{3}}}{\sqrt{3}} \int \frac{\hat{p}_s(k, k_\perp, \omega)}{(k - i0)^{\frac{2}{3}}} \, \mathrm{e}^{i(k_\perp y_3 - \frac{\pi}{3})} \, dk dk_\perp dy_3. \tag{4.11}$$

For stationary random flow we also have [3]

$$\langle \hat{p}_s(k, k_\perp, \omega) \hat{p}_s^*(k', k'_\perp, \omega') \rangle = \mathrm{P}(k, k_\perp, \omega) \delta(k - k') \delta(k_\perp - k'_\perp) \delta(\omega - \omega'), \tag{4.12}$$

where $\mathrm{P}(k, k_\perp, \omega)$ is the blocked pressure wavenumber-frequency spectrum. Hence, by forming the product $\langle \hat{F}(\omega) \hat{F}^*(\omega') \rangle$ from (4.11), using (4.12), and making the further assumption that the spanwise correlation length of the unsteady motions is small compared to the cavity width b, we deduce from the definition (4.1), that

$$\Psi(\omega) \approx \frac{8\pi C_1^2 \Gamma^2(\frac{2}{3}) b L^{\frac{2}{3}}}{3} \int_{-\infty}^{\infty} \frac{\mathrm{P}(k, 0, \omega) \, dk}{|k|^{\frac{4}{3}}}, \tag{4.13}$$

and therefore that the far field acoustic pressure spectrum (4.3) can be written

$$\Phi(\omega, \mathbf{x}) \approx \frac{4C_1^2\Gamma^2(\frac{2}{3}) b L^{\frac{2}{3}} \kappa_o^2}{3\pi(1 + M\cos\theta)^2 |\mathbf{x}|^2} \left| \frac{C_2 \sin(\kappa_o d)}{\cos\{\kappa_o(d + \ell + i\kappa_o \mathcal{A}/2\pi)\}} + i(\cos\theta - M) \right|^2 \times \int_{-\infty}^{\infty} \frac{\mathrm{P}(k, 0, \omega) \, dk}{|k|^{\frac{4}{3}}}, \quad |\mathbf{x}| \to \infty. \tag{4.14}$$

The functional form of $\mathrm{P}(k, 0, \omega)$ can in principle be estimated from measurements of the wall pressure fluctuations just downstream of the trailing edge of the cavity, provided it is permissible to assume that the statistical properties of the shear layer motions near the trailing edge of the cavity are well approximated by those immediately downstream of the cavity.

As an alternative approximate procedure, however, it will be assumed that $\mathrm{P}(k, 0, \omega)$ is sharply peaked at $k = \omega/U_c$, which is the expected behaviour when the dominant vortical disturbances convect at speed U_c. The integral in (4.14) may then be evaluated by replacing $|k|$ by ω/U_c in the denominator, and setting $\ell_3 \Phi_{pp}(\omega)/\pi = \int_{-\infty}^{\infty} \mathrm{P}(k, 0, \omega) \, dk$, where $\Phi_{pp}(\omega)$

is the frequency spectrum of the wall blocked pressure fluctuations, and $\ell_3 \ll b$ is the spanwise correlation length. Therefore,

$$\Phi(\omega,\mathbf{x}) \approx \frac{4C_1^2\Gamma^2(\frac{2}{3})bL^{\frac{2}{3}}}{3\pi^2(1+M\cos\theta)^2|\mathbf{x}|^2}\,\frac{\ell_3\kappa_o^2\Phi_{pp}(\omega)}{(\omega/U_c)^{\frac{4}{3}}}\left|\frac{C_2\sin(\kappa_o d)}{\cos\{\kappa_o(d+\ell+i\kappa_o\mathcal{A}/2\pi)\}}+\,i\,(\cos\theta-M)\right|^2,$$

$$|\mathbf{x}|\to\infty. \tag{4.15}$$

Consider a case (typical of low Mach number flow over a shallow cavity) where the pressure fluctuations near the cavity peak at the frequency of the second Rossiter mode, near $fL/U = 1$. Let the functional form of $\Phi_{pp}(\omega)$ be approximated by the following empirical formula [3] for turbulent boundary layer flow

$$\frac{\Phi_{pp}(\omega)(U/\delta_*)}{(\rho_o v_*^2)^2} \approx \frac{(\omega\delta_*/U)^2}{\{(\omega\delta_*/U)^2+\alpha_p^2\}^{\frac{3}{2}}}, \quad \alpha_p = 0.12, \quad \ell_3 \approx \frac{1.4U_c}{\omega}. \tag{4.16}$$

In this formula δ_* is the effective displacement thickness of the boundary layer flow, but will be assigned the value

$$\delta_* = \frac{L\alpha_p}{\pi\sqrt{2}}, \tag{4.17}$$

to ensure that the spectral peak occurs at $fL/U = 1$. The velocity v_* is the nominal friction velocity of the wall flow, but its precise value is not required for the present illustrations.

In non-dimensional form we may now write

$$\frac{\Phi(\omega,\mathbf{x})(U/\delta_*)}{(\rho_o v_*^2)^2(L/|\mathbf{x}|)^2}\Bigg/\frac{5.6C_1^2\Gamma^2(\frac{2}{3})}{3\pi^2}\left(\frac{\delta_*}{L}\right)^{\frac{1}{3}}\left(\frac{b}{L}\right)\left(\frac{U_c}{U}\right)^{\frac{7}{3}} \approx$$

$$\frac{M^2(\omega\delta_*/U)^{\frac{5}{3}}}{(1+M\cos\theta)^2\{(\omega\delta_*/U)^2+\alpha_p^2\}^{\frac{3}{2}}}\left|\frac{C_2\sin(\kappa_o d)}{\cos\{\kappa_o(d+\ell+i\kappa_o\mathcal{A}/2\pi)\}}+\,i\,(\cos\theta-M)\right|^2. \tag{4.18}$$

Thus, the mean square acoustic pressure scales as $(\rho_o U^2)^2M^2$, and the overall acoustic intensity varies as $\rho_o U^3M^3$. This is the expected behaviour for an aeroacoustic dipole source; in our case the source is modified by the cavity monopole, but we shall see below that the maximal strength of the monopole is of the same dipole order.

Typical plots of the far field acoustic spectrum

$$10\times\log_{10}\left\{\frac{\Phi(\omega,\mathbf{x})(U/\delta_*)}{(\rho_o v_*^2)^2(L/|\mathbf{x}|)^2}\Bigg/\frac{5.6C_1^2\Gamma^2(\frac{2}{3})}{3\pi^2}\left(\frac{\delta_*}{L}\right)^{\frac{1}{3}}\left(\frac{b}{L}\right)\left(\frac{U_c}{U}\right)^{\frac{7}{3}}\right\}$$

are illustrated in Figures 3 and 4 respectively for $M = 0.01,\ 0.1$ in the radiation direction $\theta = 30°$. It is assumed that

$$\frac{U_c}{U} = 0.5, \quad \frac{b}{L} = 1, \quad \frac{d}{L} = 0.5, \quad \text{for which} \quad C_1 = 0.69, \quad C_2 = 1.02. \tag{4.19}$$

Also shown for comparison is the model shear layer mode blocked pressure spectrum Φ_{pp} normalized as in (4.16), with a broad peak at the second Rossiter frequency ($fL/U \approx 1$).

The very low Mach number case $M = 0.01$ is characteristic of underwater applications, provided the cavity walls are sufficiently rigid that structurally driven cavity modes are not important. The monopole peak occurs at the relatively high Strouhal number $fL/U \sim 25$, and its contribution is smaller than that of the spectrum maximum near the Rossiter mode $fL/U = 1$. At Strouhal numbers less than 10 the radiation is dominated by the drag dipole source – Mach number ('Döppler') effects are unimportant when $M = 0.01$, and this implies that the radiation directivity has the usual dipole peaks in the upstream and downstream directions, and that there is a radiation null in the direction normal to the wall. In practice the source spectrum Φ_{pp} probably decays much faster than the boundary layer analog model (4.16) used in this calculation, and this would tend to suppress even further the higher frequency monopole radiation.

The situation is very different at the higher Mach number $M = 0.1$ (Figure 4). The cavity mode resonance frequency $fL/U \sim 2.5$, and the monopole peak is several dB above the dipole peak at the Rossiter frequency ($fL/U = 1$), although it should be observed that the magnitude of this peak scales approximately in proportion to $(\rho_o U^2)^2 M^2$, as for the dipole sound. The presence of this peak in the lower frequency region has a profound effect on the radiation directivity, as indicated in Figure 5, in which the magnitude of

$$\frac{\Phi(\omega, \mathbf{x})(U/\delta_*)}{(\rho_o v_*^2)^2 (L/|\mathbf{x}|)^2}$$

is plotted against the radiation direction θ for $fL/U = 0.5,\ 1,\ 1.5,\ 2,\ 2.5$, all curves being to the same scale. In Figure 4 it can be seen that the lowest frequency $fL/U = 0.5$ is sufficiently far from the monopole peak to be effectively uninfluenced by the monopole. The directivity is therefore that of a dipole, peaking in the upstream and downstream directions, but subject to Döppler amplification by the mean flow, which causes the level to be larger in upstream directions. The dotted curves in Figures 3 and 4 represent the field of the monopole cavity mode alone, when the term $i(\cos\theta - M)$ on the right of (4.18) is deleted. This shows that the influence of the monopole is confined to the immediate vicinity of the

resonance frequency. At higher frequencies the detailed directivity is determined by phase interference between the monopole and dipole, as well as the differences in the Döppler effects on both sources. Thus, at the spectral peak at $fL/U = 2.5$ this interference produces strong radiation preferentially in the downstream direction.

An overall picture of the far field radiation is obtained by integrating the spectrum (4.18) with respect to ω. The integral is convergent at $\omega = +\infty$, but contributions at very high frequencies are probably not representative. Therefore we depict in Figure 6 for $M = 0.05,\ 0.1$ the radiated pressure directivity when the integration is confined to the Strouhal number range $0.1 < fL/U < 10$. In both cases this includes the frequency range in which the monopole is important. At the lower Mach number the directivity resembles that of a dipole, but peaking in the downstream direction owing to modifications produced by the monopole resonant response. The situation at $M = 0.1$ is similar except that there is significant radiation in directions normal to the wall.

5. CONCLUSION

At very low Mach numbers the aerodynamic sound generated by nominally steady flow over a shallow wall cavity is dominated by dipole radiation produced by the unsteady drag force, the radiation peaking in directions upstream and downstream of the cavity. The drag force fluctuations are produced by the interaction of vorticity, in an unstable mean shear layer or periodically ejected from the cavity, with the trailing edge of the cavity. It is the principal source in underwater applications where M rarely exceeds about 0.01, provided it is permissible to ignore structural resonances associated with hydrodynamic forcing of flexing cavity walls. In such cases the lowest, rigid body cavity resonance frequency (the 'Helmholtz' resonance frequency) tends to be large, and beyond the range where it can be effectively excited by the flow. At higher Mach numbers, however, the resonance frequency lies closer to the relevant 'Rossiter' modes of the unstable hydrodynamic flow over the cavity, and can then make a significant contribution to the radiation.

The cavity resonance produces a monopole contribution to the sound and is governed by compressible effects in the cavity region. At low Mach numbers these are usually very weak, such that whereas the intensity of the drag dipole exhibits the usual aeroacoustic dipole strength $\sim \rho_o U^3 M^3$, the strength of the compressible-dominated, cavity source would vary as $\sim \rho_o U^3 M^5$. However, when significant excitation of the cavity resonance occurs, say at Mach numbers exceeding about 0.05, the unsteady drag fluctuations also excite the cavity mode with a radiation intensity of the same order as the dipole sound. At these higher Mach numbers the radiation directivity at a frequency close to the cavity resonance is governed by the correlated interference between the dipole and monopole fields; at frequencies far removed from the resonance the directivity reverts to that of an isolated dipole. The overall sound power now tends to be uniformly distributed in direction; in particular there is significant radiation in the direction normal to the wall, which is otherwise a radiation null for the dipole alone.

The detailed results given in this chapter are for a moderately shallow cavity dominated by shear layer mode instabilities, of the kind usually associated with the Rossiter modes. However, the Green's function developed in §3 can also be used to determine the cavity radiation for very shallow cavities, where an unsteady hydrodynamic 'wake flow' wets the cavity base, and the motion is characterized by the quasi-periodic ejection of cavity vorticity into the main flow. This ejection produces a violent fluctuation in the drag, which determines both the dipole and monopole sources of sound.

REFERENCES

1. J. E. Rossiter 1962 The effect of cavities on the buffeting of aircraft. *Royal Aircraft Establishment Tech. Memo.* 754.
2. M. S. Howe 1997 Edge, cavity and aperture tones at very low Mach numbers. *Journal of Fluid Mechanics* **330**, 61 - 84.
3. M. S. Howe 1998 *Acoustics of fluid-structure interactions*, Cambridge University Press.
4. D. Rockwell 1983 Oscillations of impinging shear layers. *American Institute of Aeronautics and Astronautics Journal* **21**, 645 - 664.
5. N. M. Komerath, K. K. Ahuja and F. W. Chambers 1987 *American Institute of Aeronautics and Astronautics* Paper 87-022. Prediction and measurement of flows over cavities - a survey.
6. K. K. Ahuja and J. Mendoza 1995 NASA Contractor Report 4653: Final Report Contract NAS1-19061, Task 13. *Effects of cavity dimensions, boundary layer, and temperature on cavity noise with emphasis on benchmark data to validate computational aeroacoustic codes.*
7. D. Rockwell and E. Naudascher 1978 Review - self-sustaining oscillation of flow past cavities. *Transactions of the American Society of Mechanical Engineers, Journal of Fluids Engineering* **100**, 152 - 165.
8. S. M. Grace 2001 *American Institute of Aeronautics and Astronautics* Paper 2001 - 0510. An overview of computational aeroacoustic techniques applied to cavity noise prediction.
9. M. Gharib and A. Roshko 1987 The effect of flow oscillations on cavity drag. *Journal of Fluid Mechanics* **177**, 501 - 530.
10. T. Colonius, A. Basu and C. Rowley 1999 *American Institute of Aeronautics and Astronautics* Paper 99-1912. Numerical investigation of flow past a cavity.
11. D. F. Fuglsang and A. B. Cain 1992 *American Institute of Aeronautics and Astronautics* Paper 92-0555. Evaluation of shear layer cavity resonances by numerical simulation.
12. C. K. W. Tam and P. J. W. Block 1978 On the tones and pressure oscillations induced by flow over rectangular cavities. *Journal of Fluid Mechanics* **89**, 373 - 399.

13. X. Zhang 1995 *American Institute of Aeronautics and Astronautics Journal* **33**, 1404 - 1411. Compressive cavity flow oscillations due to shear layer instabilities and pressure feedback.

14. H. E. Plumblee, J. S. Gibson and L. W. Lassiter 1962 *A theoretical and experimental investigation of the acoustic response of cavities in an aerodynamic flow.* U. S. Air Force Report WADD-TR-61-75.

15. L. F. East 1966 Aerodynamically induced resonance in rectangular cavities. *Journal of Sound and Vibration* **3**, 277 - 287.

16. Y. H. Yu 1976 *American Institute of Aeronautics and Astronautics* Paper 76-529. Measurements of sound radiation from cavities at subsonic speeds.

17. M. Inagaki, O. Murata and T. Kondoh 2002 *American Institute of Aeronautics and Astronautics Journal* **40**, 1821 - 1829. Numerical prediction of fluid-resonant oscillation at low Mach number.

18. M. Jacob, V. Gradoz, A. Louisot, S. Juve and S. Guerrand. 1999 *American Institute of Aeronautics and Astronautics* Paper 99-1892. Comparison of sound radiated by shallow cavities and backward facing steps.

19. J. C. Hardin and D. S. Pope 1994 An acoustic/viscous splitting technique for computational aeroacoustics. *Theoretical and Computational Aeroacoustics* **6**, 323 - 340.

20. J. C. Hardin and D. S. Pope 1995 *American Institute of Aeronautics and Astronautics Journal* **33**, 407 - 412. Sound generation by flow over a two-dimensional cavity.

21. J. A. Ekaterinaris 1999 *American Institute of Aeronautics and Astronautics Journal* **37**, 1033 - 1039. New formulation of Hardin - Pope equations for aeroacoustics.

22. W. Z. Shen and J. N. Sorensen 1999 *American Institute of Aeronautics and Astronautics Journal* **37**, 141 - 143. Comment on the aeroacoustic formulation of Hardin and Pope.

23. S. M. Grace and C. K. Curtis 1999 Acoustic computations using incompressible inviscid CFD results as input, *Proceedings of the ASME Noise Control and Acoustics Division* (NCA-Vol 26) ASME IMECE, Nashville, TN, November 1999.

24. C. Curtis Granda 2001 *A computational acoustic prediction method applied to two-dimensional cavity flow*, Master's Thesis, Boston University, December, 2001.

25. G. K. Batchelor 1967 *An Introduction to Fluid Dynamics,* Cambridge University Press.

26. K. Taylor 1978 A transformation of the acoustic equation with implications for wind tunnel and low speed flight tests. *Proceedings of the Royal Society of London* **A363**, 271 - 281.

27. Lord Rayleigh 1945 *Theory of Sound*, Volume 2. New York: Dover.

28. Horace Lamb 1932 *Hydrodynamics* (6th. ed.). Cambridge University Press.

29. C. K. W. Tam 1976 The acoustic modes of a two-dimensional rectangular cavity. *Journal of Sound and Vibration* **49**, 353 - 364.

30. M. S. Howe 1976 The influence of vortex shedding on the generation of sound by convected turbulence. *Journal of Fluid Mechanics* **76**, 711 - 740.

31. D. G. Crighton 1985 The Kutta condition in unsteady flow. *Annual Reviews of Fluid Mechanics* **17**, 411 - 445.

32. T. Takaishi, A. Sagawa, K. Nagakura and T. Maeda 2002 Numerical analysis of dipole sound source around high speed trains. *Journal of the Acoustical Society of America* **111**, 2601 - 2608.

33. M. Abramowitz and I. A. Stegun (editors) 1970 *Handbook of Mathematical Functions* (Ninth corrected printing), US Department of Commerce, National Bureau of Standards Applied Mathematics Series No.55.

34. D. G. Crighton 1975 Scattering and diffraction of sound by moving bodies. *Journal of Fluid Mechanics* **72**, 209 - 227.

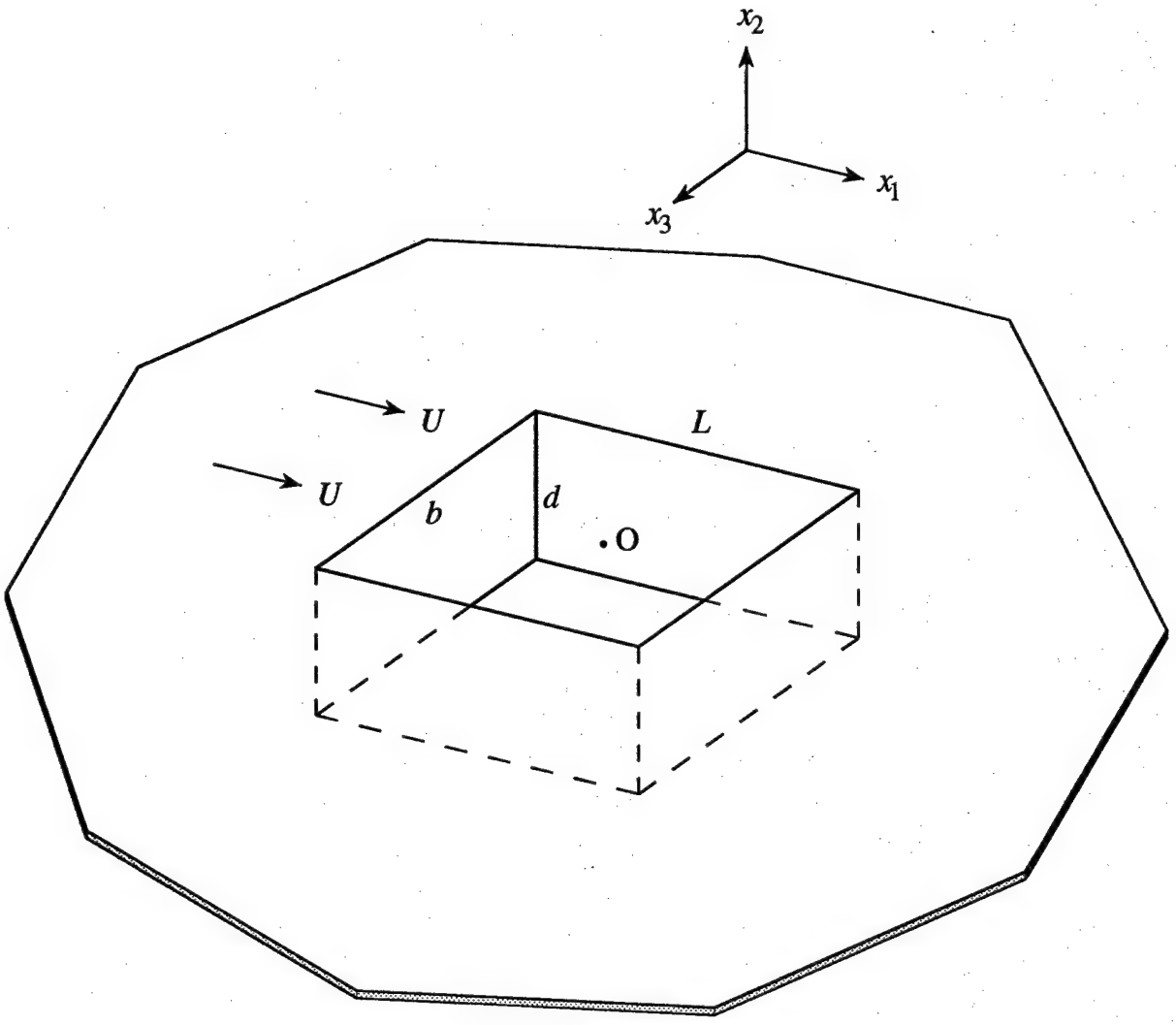

Figure 1. Schematic configuration of nominally steady, high Reynolds number flow over a rigid, rectangular wall cavity of depth d and streamwise length L.

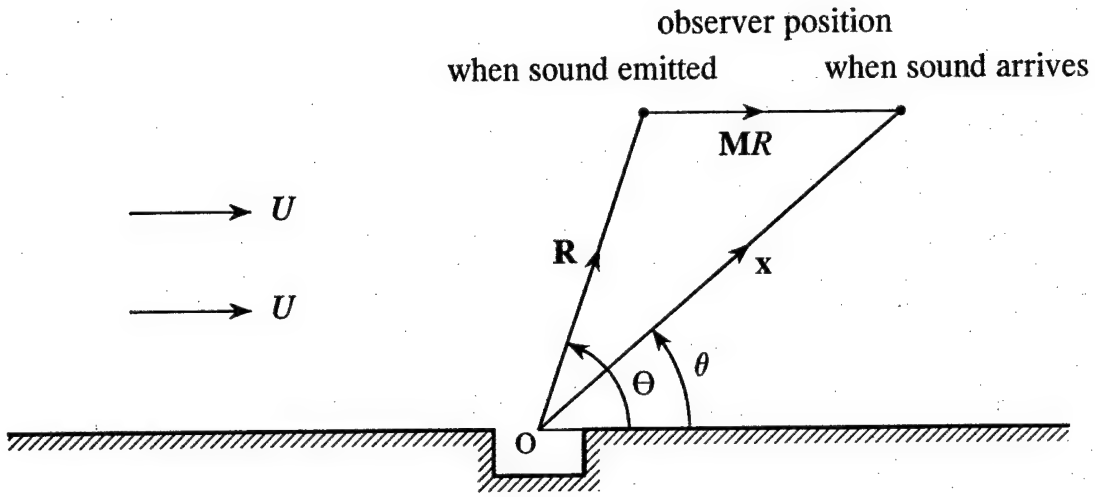

Figure 2. Illustrating the relation between the coordinate systems $\mathbf{x}$ and $\mathbf{R}$.

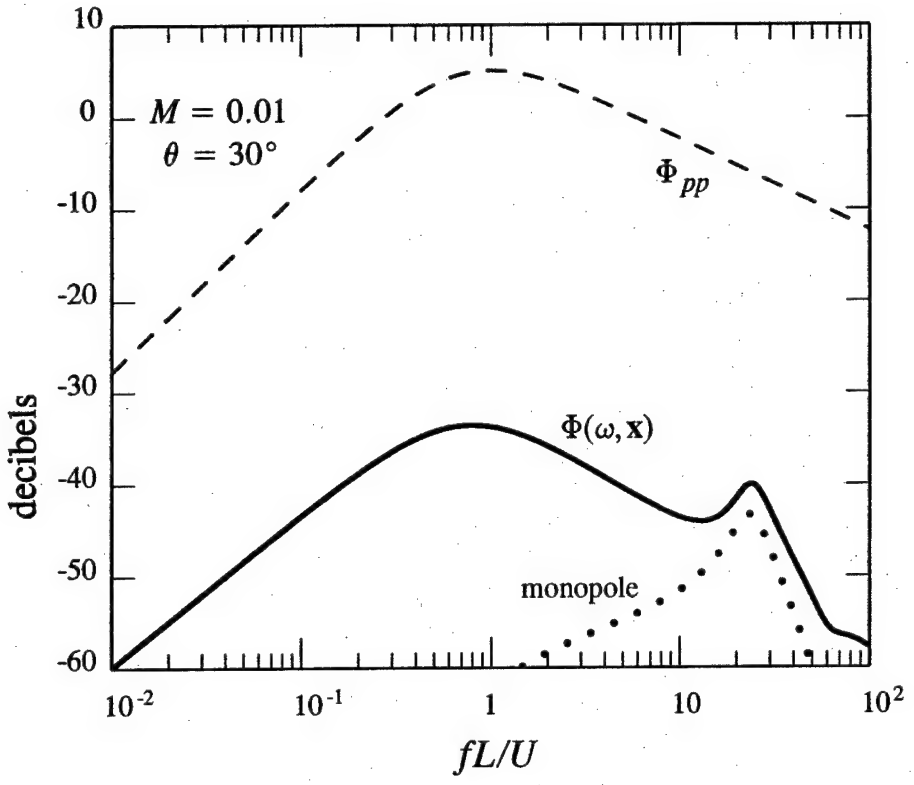

Figure 3. Acoustic pressure spectrum

$$10 \times \log_{10} \left\{ \frac{\Phi(\omega, \mathbf{x})(U/\delta_*)}{(\rho_o v_*^2)^2 (L/|\mathbf{x}|)^2} \Big/ \frac{5.6 C_1^2 \Gamma^2(\frac{2}{3})}{3\pi^2} \left(\frac{\delta_*}{L}\right)^{\frac{1}{3}} \left(\frac{U_c}{U}\right)^{\frac{7}{3}} \right\}$$

(———) defined by (4.18) for conditions (4.19) when $M = 0.01$, $\theta = 30°$. Also shown is the corresponding blocked pressure spectrum $10 \times \log_{10}\left(\Phi_{pp}(U/\delta_*)/(\rho_o v_*^2)^2\right)$ (- - - -, equation (4.16)) peaking at the second Rossiter mode $fL/U \sim 1$, and the cavity 'monopole' radiation (• • •).

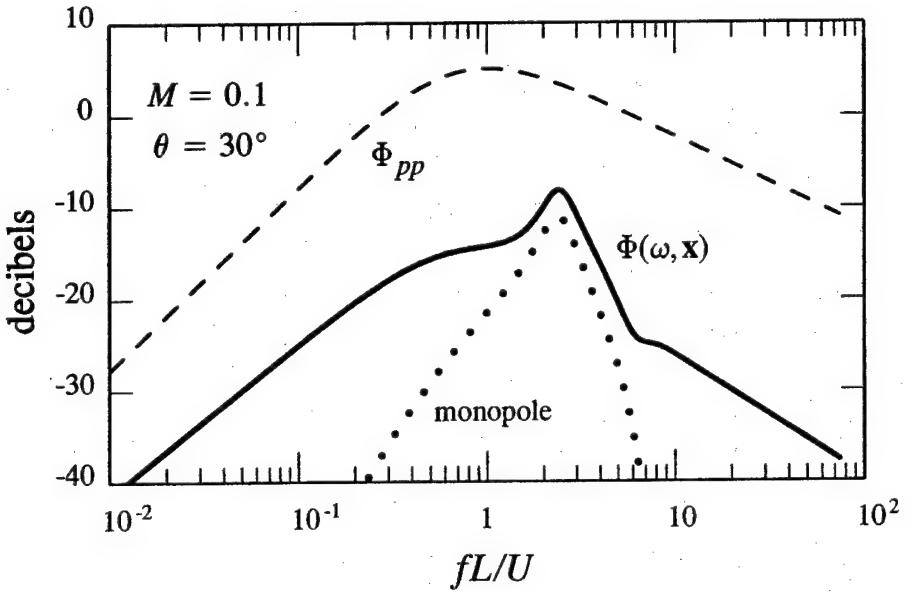

Figure 4. Acoustic pressure spectrum

$$10 \times \log_{10} \left\{ \frac{\Phi(\omega, \mathbf{x})(U/\delta_*)}{(\rho_o v_*^2)^2 (L/|\mathbf{x}|)^2} \Big/ \frac{5.6 C_1^2 \Gamma^2(\frac{2}{3})}{3\pi^2} \left(\frac{\delta_*}{L}\right)^{\frac{1}{3}} \left(\frac{U_c}{U}\right)^{\frac{7}{3}} \right\}$$

(———) defined by (4.18) for conditions (4.19) when $M = 0.1$, $\theta = 30°$. Also shown is the corresponding blocked pressure spectrum $10 \times \log_{10}\left(\Phi_{pp}(U/\delta_*)/(\rho_o v_*^2)^2\right)$ (- - - -, equation (4.16)) peaking at the second Rossiter mode $fL/U \sim 1$, and the cavity 'monopole' radiation (• • •).

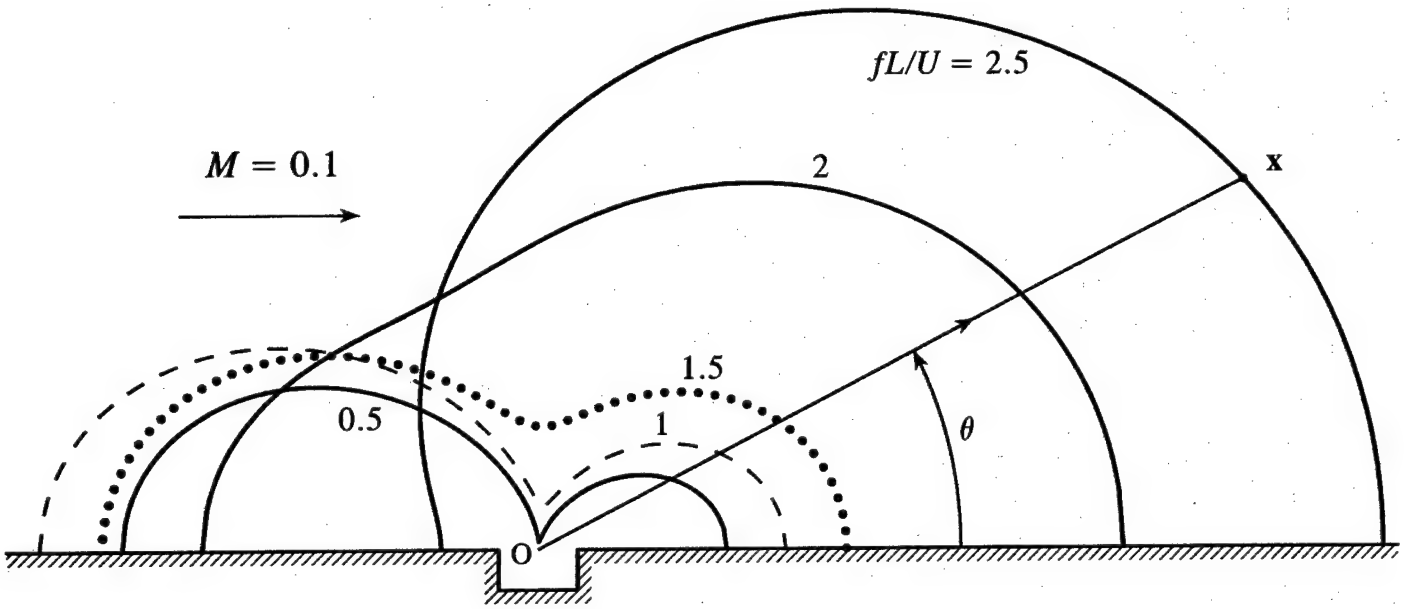

Figure 5. Directivity

$$\frac{\Phi(\omega, \mathbf{x})(U/\delta_*)}{(\rho_o v_*^2)^2 (L/|\mathbf{x}|)^2}$$

for a cavity of dimensions (4.19) for $M = 0.1$ and $fL/U = 0.5,\ 1,\ 1.5,\ 2,\ 2.5$ when the shear layer blocked pressure spectrum Φ_{pp} peaks at the second Rossiter mode $fL/U \sim 1$.

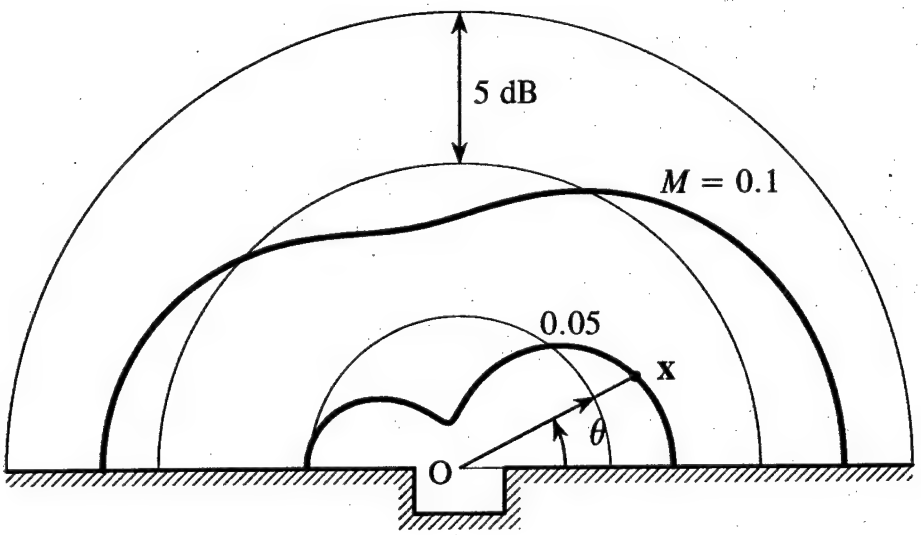

Figure 6. Directivity $10 \times \log_{10}(\langle p^2(\mathbf{x},t)\rangle/p_0^2)$ of overall sound radiated in the frequency range $0.1 < fL/U < 10$ for $M = 0.05,\ 0.1$ for the cavity defined by (4.19).

CHAPTER 2

WALL-CAVITY ACOUSTIC GREEN'S FUNCTION AT LOW MACH NUMBER

SUMMARY

Analytical approximations are developed for the low Mach number, aeroacoustic Green's function for a rectangular or circular cylindrical open cavity in a plane, rigid wall. The formulae can be used to predict the sound radiated into the main flow from a knowledge of the hydrodynamic flow near the cavity. At low Mach numbers the sound is a small by-product of the main flow, whose hydrodynamic properties can first be determined from observation or from a numerical treatment of the incompressible Navier-Stokes equations. Detailed predictions are made of the lowest order, open cavity resonance frequencies, and it is shown how a resonance is excited by the unsteady drag, and also by the lift or drag force experienced by a small bluff body placed in the flow close to the cavity. The cavity resonance frequencies are complex, with imaginary parts depending primarily on radiation damping, which can be sufficiently large for a shallow, open cavity, that a distinct resonance peak is absent from the acoustic spectrum – for a square cavity such peaks are predicted only when the cavity depth exceeds about half the cavity length. For very shallow cavities the efficiency of sound production by volumetric pulsations within the cavity is comparable to that of free field turbulence quadrupoles, and therefore negligible at low Mach numbers.

1. INTRODUCTION

The sound produced by nominally steady flow at low Mach number M past a shallow wall cavity can be attributed to the combined fields of a monopole and a dipole source (see [1, 2] and references cited therein). The dipole strength is equal to the unsteady drag, and the dipole radiation peaks in directions upstream and downstream of the cavity. It dominates the production of sound at very low Mach numbers, $M \ll 0.1$, say, and is therefore the most important source in an underwater flow ($M \sim 0.01$) over a cavity whose walls may be regarded as 'hydraulically rigid' (so that monopole sources generated by flexing of the cavity walls are absent). At higher Mach numbers ($M \sim 0.1$) unsteady forces on the downstream cavity wall excite the low order cavity depth (or 'Helmholtz') mode, which behaves as a monopole source. The monopole sound can exceed or be comparable to the dipole radiation over a range of frequencies close to resonance.

Approximate formulae for calculating the radiation in terms of an assumed knowledge of the vorticity distribution near the cavity (or, equivalently, in terms of the fluctuating drag) were given in [2]. For a shallow rectangular cavity of depth d and streamwise length L (Figure 1), the resonant oscillations governing the monopole are heavily damped by radiation losses when d/L is smaller than 0.5. The damping and resonance frequencies vary significantly with d/L, and one of the objectives of the present chapter is to determine this dependence for typical cavities of rectangular and circular cross-sections, and to obtain corresponding explicit representations of the cavity acoustic Green's function that can be used to calculate the sound generated by flow-cavity interaction at low Mach numbers.

To do this we shall consider first sound production by a point source at $\mathbf{y}$ near the wall cavity of Figure 1 in the presence of a low Mach number, high Reynolds number mean flow at speed U in the positive x_1-direction of the rectangular coordinates (x_1, x_2, x_3), where both the wall and the cavity-interior surfaces are rigid. The coordinate origin is taken at O in the plane of the wall at the centre of the cavity, with the x_2-axis normal to the wall and directed into the main stream. For this ideal situation the point source is the only source of sound, so that the flow elsewhere must be irrotational. In particular the mean flow past the cavity must be regarded as irrotational, with steady mean velocity $\mathbf{U}_o = \mathbf{U}_o(\mathbf{x})$, say, where $\mathbf{U}_o \to (U, 0, 0)$ at large distances from the cavity.

When $M^2 \ll 1$ the mean fluid density ρ_o and sound speed c_o may be taken to be constant throughout the flow [3]. To first order in $M = U/c_o$, the acoustic wave equation for the

unsteady component $\varphi(\mathbf{x}, t)$ of the velocity potential is then governed by [4, 5]

$$\left\{\frac{1}{c_o^2}\left(\frac{\partial^2}{\partial t^2} + 2\mathbf{U_o}\cdot\nabla\frac{\partial}{\partial t}\right) - \nabla^2\right\}\varphi = 0, \tag{1.1}$$

subject to

$$\frac{\partial\varphi}{\partial x_n} = 0 \ \text{ on } \ \mathrm{S}, \tag{1.2}$$

where S denotes the rigid surface formed by the wall $x_2 = 0$ and cavity-interior surfaces, and x_n is measured in the normal direction on S into the fluid. The Green's function $G(\mathbf{x}, \mathbf{y}, t-\tau)$ is the solution with outgoing wave behaviour of

$$\left\{\frac{1}{c_o^2}\left(\frac{\partial^2}{\partial t^2} + 2\mathbf{U_o}\cdot\nabla\frac{\partial}{\partial t}\right) - \nabla^2\right\}G = \delta(\mathbf{x}-\mathbf{y})\delta(t-\tau), \tag{1.3}$$

where $\partial G/\partial x_n = 0$ on S.

Functional forms for G are determined in this chapter for shallow cavities, incorporating the cavity monopole and dipole contributions. Details are given in Section 2 for a rectangular cavity, and summarized for the circular cylindrical cavity in Section 3. Application is made in Section 4 to determine the influence on cavity mode excitation of a bluff body in the main stream adjacent to the cavity mouth. It is shown how the open cavity Green's function can be modified to account for the presence of a body whose streamwise dimensions are small relative to the cavity diameter. It is also shown how the efficiency of cavity mode excitation rapidly decreases with decreasing cavity depth.

The chapter is dedicated to Professor Alan Powell, who pioneered the theoretical and experimental study of the production of aerodynamic sound by low Mach number periodic flows [6].

2. THE RECTANGULAR WALL CAVITY

2.1 Taylor's transformation

The irrotational mean velocity $\mathbf{U}_o(\mathbf{x})$ may be assumed to be incompressible when the Mach number is sufficiently small that M^2 can be neglected relative to unity [3]. Its behaviour near the cavity depends on cavity geometry, and can be expressed in the form

$$\mathbf{U}_o = \nabla\{\mathbf{U}\cdot\mathbf{X}(\mathbf{x})\}, \quad \mathbf{U} = (U,0,0), \tag{2.1}$$

where $\mathbf{X}(\mathbf{x}) = (X_1(\mathbf{x}), 0, X_3(\mathbf{x}))$ is the wall cavity 'Kirchhoff vector' whose component X_j $(j = 1, 3)$ satisfies

$$\nabla^2 X_j = 0, \quad X_j \to x_j \ \text{ as } |\mathbf{x}| \to \infty, \ \ \frac{\partial X_j}{\partial x_n} = 0 \text{ on S.} \tag{2.2}$$

$X_j(\mathbf{x})$ $(j = 1, 3)$ is the velocity potential of flow over the wall and cavity that has unit speed in the j-direction at large distances from the cavity.

The Green's function equation (1.3) is simplified at low Mach numbers by making Taylor's transformation [4, 5]

$$G(\mathbf{x},\mathbf{y},t-\tau) = -\frac{1}{2\pi}\int_{-\infty}^{\infty}\hat{G}(\mathbf{x},\mathbf{y},\omega)\mathrm{e}^{-i\omega(t-\tau+\mathbf{M}\cdot(\mathbf{X}-\mathbf{Y})/c_o)}d\omega, \tag{2.3}$$

where $\mathbf{M} = \mathbf{U}/c_o$, and $\mathbf{Y} = (Y_1, 0, Y_3)$ is the Kirchhoff vector expressed in terms of $\mathbf{y}$. When terms $\sim O(M^2)$ and smaller are systematically neglected, $\hat{G}$ is found to satisfy

$$\left(\nabla^2 + \kappa_o^2\right)\hat{G} = \delta(\mathbf{x}-\mathbf{y}), \quad \frac{\partial\hat{G}}{\partial x_n} = 0 \text{ on S,} \tag{2.4}$$

where $\kappa_o = \omega/c_o$ is the acoustic wavenumber.

In aeroacoustic applications the source point $\mathbf{y}$ is near or within the cavity and the observer is at $\mathbf{x}$ in the acoustic far field. It is then usual to solve (2.4) using the reciprocal theorem $\hat{G}(\mathbf{x},\mathbf{y},\omega) = \hat{G}(\mathbf{y},\mathbf{x},\omega)$ [7]: the source on the right of (2.4) is regarded as placed at the distant, far field point $\mathbf{x}$, and the reciprocal equation is solved for $\hat{G}(\mathbf{y},\mathbf{x},\omega)$ *as a function of* $\mathbf{y}$ in the neighbourhood of the cavity, with $\partial\hat{G}(\mathbf{y},\mathbf{x},\omega)/\partial y_n = 0$ on S. The distant source generates a spherical wave with potential $-\mathrm{e}^{i\kappa_o|\mathbf{x}-\mathbf{y}|}/4\pi|\mathbf{x}-\mathbf{y}|$. When the presence of the cavity is ignored the velocity potential near the wall is obtained by augmenting this spherical wave by the potential $-\mathrm{e}^{i\kappa_o|\bar{\mathbf{x}}-\mathbf{y}|}/4\pi|\bar{\mathbf{x}}-\mathbf{y}|$ produced by an equal

image source at $\bar{\mathbf{x}} = (x_1, -x_2, x_3)$. The net velocity potential $\hat{G}_0(\mathbf{y}, \mathbf{x}, \omega)$, say, 'incident' on the cavity may therefore be approximated (as a function of $\mathbf{y}$) by

$$\hat{G}_0(\mathbf{y}, \mathbf{x}, \omega) \approx -\frac{e^{i\kappa_0|\mathbf{x}|}}{4\pi|\mathbf{x}|}\left(e^{-i\kappa_o \mathbf{n}\cdot\mathbf{y}} + e^{-i\kappa_o \mathbf{n}\cdot\bar{\mathbf{y}}}\right), \quad |\mathbf{x}| \to \infty, \text{ where } \mathbf{n} = \frac{\mathbf{x}}{|\mathbf{x}|}, \ \bar{\mathbf{y}} = (y_1, -y_2, y_3). \tag{2.5}$$

To complete the determination of $\hat{G}(\mathbf{y}, \mathbf{x}, \omega)$ it remains to calculate the interaction of $\hat{G}_0$ with the cavity.

2.2 Contribution from cavity oscillations

In typical low Mach number flows the wavelengths of flow-generated sound will be comparable to, or much larger than, the cavity diameter. This is necessary for the effective excitation of low order cavity resonances, whose motions are well correlated over the cavity mouth. When this happens the incident disturbance (2.5) will induce a gross reciprocating flow across the plane of the mouth with mean normal velocity $u_c \equiv u_c(\kappa_o)$, say, corresponding to the excitation of a cavity depth mode $\hat{G}_c$, where

$$\hat{G}_c = -\frac{u_c \cos\left(\kappa_o(y_2 + d)\right)}{\kappa_o \sin(\kappa_o d)}, \quad -d < y_2 < 0. \tag{2.6}$$

The motion produced above the cavity (in $y_2 > 0$) by the cavity oscillation (with vanishing normal derivative on the wall outside the cavity) can be written

$$\hat{G}_c = \iint_{-\infty}^{\infty} \frac{\mathcal{U}(k_1, k_3)}{i\sqrt{\kappa_o^2 - k^2}} e^{i\left(k_1 y_1 + k_3 y_3 + y_2\sqrt{\kappa_o^2 - k^2}\right)} dk_1 dk_3, \quad k^2 = k_1^2 + k_3^2, \tag{2.7}$$

where for real κ_0 and k branch-cuts for $\sqrt{\kappa_o^2 - k^2}$ are chosen such that

$$\sqrt{\kappa_o^2 - k^2} = \begin{cases} \operatorname{sgn}(\kappa_o)|\kappa_o^2 - k^2|^{\frac{1}{2}} & \text{for } \kappa_o^2 > k^2, \\ +i|\kappa_o^2 - k^2|^{\frac{1}{2}} & \text{for } \kappa_o^2 < k^2. \end{cases} \tag{2.8}$$

$\mathcal{U}(k_1, k_3)$ is the Fourier transform of the normal velocity in the plane of the wall. When $\kappa_o L \sim O(1)$ or smaller, a good first approximation is obtained by replacing the open face of the cavity by a massless piston, in which case

$$\mathcal{U}(k_1, k_3) = \frac{u_c}{(2\pi)^2} \int_{-\frac{L}{2}}^{\frac{L}{2}} e^{-ik_1 y_1} dy_1 \int_{-\frac{b}{2}}^{\frac{b}{2}} e^{-ik_3 y_3} dy_3 = \frac{u_c \mathcal{A}}{(2\pi)^2} \mathcal{S}\left(\frac{k_1 L}{2}\right) \mathcal{S}\left(\frac{k_3 b}{2}\right), \tag{2.9}$$

where $\mathcal{A} = bL$ is the cavity open area, and $\mathcal{S}(x) \equiv \sin(x)/x$, and therefore

$$\hat{G}_c = \frac{u_c \mathcal{A}}{i(2\pi)^2} \iint_{-\infty}^{\infty} \frac{\mathcal{S}(k_1 L/2)\mathcal{S}(k_3 b/2)}{\sqrt{\kappa_o^2 - k^2}} \, \mathrm{e}^{i\left(k_1 y_1 + k_3 y_3 + y_2\sqrt{\kappa_o^2 - k^2}\right)} dk_1 dk_3, \quad y_3 > 0. \tag{2.10}$$

This formula for a baffled, rectangular piston is given by Morse and Ingard [8].

The piston velocity u_c is found by equating the mean (surface averaged) potentials at $y_2 = \pm 0$, just above and below the cavity opening:

$$-\frac{u_c \cos(\kappa_o d)}{\kappa_o \sin(\kappa_o d)} = \frac{1}{\mathcal{A}} \int_{-\frac{L}{2}}^{\frac{L}{2}} dy_1 \int_{-\frac{b}{2}}^{\frac{b}{2}} \left(\hat{G}_0 + \hat{G}_c\right)_{y_2 = +0} dy_3, \tag{2.11}$$

where in the integral $\hat{G}_0$, $\hat{G}_c$ are given respectively by (2.5) and (2.10). This yields

$$u_c = \frac{\kappa_o \sin(\kappa_o d)\mathcal{S}(\kappa_o L n_1/2)\mathcal{S}(\kappa_o b n_3/2)}{\{\cos(\kappa_o d) - \sin(\kappa_o d)\mathcal{F}(\kappa_o L/2)\}} \cdot \frac{\mathrm{e}^{i\kappa_o|\mathrm{x}|}}{2\pi|\mathrm{x}|}, \tag{2.12}$$

where

$$\mathcal{F}(\mu) = \frac{i\alpha\mu}{\pi^2} \int_0^{\infty} \frac{\lambda \, d\lambda}{\sqrt{\mu^2 - \lambda^2}} \int_0^{2\pi} \mathcal{S}^2(\lambda \cos\vartheta)\mathcal{S}^2(\alpha\lambda \sin\vartheta) \, d\vartheta, \quad \alpha = \frac{b}{L}. \tag{2.13}$$

The function $\mathcal{F}(\mu)$ is proportional to the complex radiation impedance of a rectangular piston in a plane wall [8].

2.3 Lowest order cavity resonance

For a shallow cavity ($d/L \ll 1$) only the lowest order depth mode is likely to be significantly excited at low Mach numbers. The resonance frequencies correspond to zeros κ_o of denominator in (2.12). By hypothesis, the Green's function describes an entirely irrotational disturbance (produced by the point source) of the irrotational mean flow $\mathbf{U}_o$ past the cavity; the motion is necessarily stable and the zeros must therefore lie exclusively in the lower half of the complex κ_o-plane.

Introduce the notations

$$z = \kappa_o d, \quad X = \frac{L}{2d}. \tag{2.14}$$

Then the complex resonance frequencies are the roots of

$$\cos z - \mathcal{F}(\mu)\sin z = 0, \quad \text{where} \quad \mu = Xz. \tag{2.15}$$

When the cavity aspect ratio $\alpha = b/L$ is fixed, equation (2.15) determines z as a function $z(X)$ of $X = L/2d$, and the change dz in such a root produced by a change dX in X satisfies

$$\frac{dz}{dX} = \frac{-z\mathcal{F}'(\mu)}{\operatorname{cosec}^2 z + X\mathcal{F}'(\mu)} \tag{2.16}$$

where $\mathcal{F}'(\mu) \equiv d\mathcal{F}(\mu)/d\mu$ is given by

$$\mathcal{F}'(\mu) = -\frac{i\alpha}{\pi^2}\int_0^\infty \frac{\lambda^3\, d\lambda}{(\mu^2-\lambda^2)^{\frac{3}{2}}}\int_0^{2\pi} \mathcal{S}^2(\lambda\cos\vartheta)\mathcal{S}^2(\alpha\lambda\sin\vartheta)\, d\vartheta. \tag{2.17}$$

But $\mathcal{F}(\mu) \to 0$ as $X \to 0$, in which case the nondimensional resonance frequencies revert to $z_n^0 = (n-\frac{1}{2})\pi$, $n = 0,\ \pm1,\ \pm2,\ \pm3,\ \ldots$, for a long tube open at one end. The corresponding value of the nth root z_n for $X > 0$ can therefore be found by numerical integration of (2.16) (using, say, a standard Runge-Kutta algorithm) subject to the initial condition

$$z = z_n^o \equiv \left(n - \frac{1}{2}\right)\pi \quad \text{at} \quad X = 0. \tag{2.18}$$

To do this the integral (2.17) must be evaluated numerically. The square root $\sqrt{\mu^2-\lambda^2}$ in the integrand is defined as in (2.8) for real values of $\mu = X\kappa_o d$ and $\lambda = Xkd$. This means that (for real $\mu > 0$) a branch cut may be assumed to extend from $\lambda = \mu$ to $\lambda = +i\infty$ in the upper half of the complex λ-plane. Now $\mu = z(X)X$ travels along a path from the origin into the lower half-plane when equation (2.16) is integrated from $X = 0$ into $X > 0$. The branch point at $\lambda = \mu$ therefore moves into $\operatorname{Im}\lambda < 0$, requiring the contour for the λ-integration to be displaced down into the lower half-plane, so that it always passes below $\lambda = \mu$. This is illustrated in Figure 2, which shows a typical trajectory of the branch point μ for $n = 1$; also shown is the integration contour used in these calculations, which was fixed and defined parametrically by

$$\lambda = t\left(1 - is\,\mathrm{e}^{-t/t_o}\right), \quad 0 < t < +\infty, \tag{2.19}$$

where $s = 3.5$ and $t_o = 1.5$. The contour passes below $\lambda = \mu$ for $0 < X < 20$ (corresponding to $0.025 < d/L < \infty$).

The trajectories of the nondimensional complex resonance frequency $\kappa_o L \equiv \omega L/c_o$ calculated by numerical integration of (2.16) for a range of values of the cavity depth ratio d/L are plotted in Figure 3 for the lowest order depth mode ($n = 1$), and for the aspect ratios $\alpha \equiv b/L = 0.5,\ 1,\ 2$. The figure reveals the progressively important role of radiation

damping with decreasing values of the cavity depth d, evidenced by the corresponding rapid increase in magnitude of the imaginary part of $\kappa_o L$. This conclusion is confirmed by the numerical results in Table 1 for $b/L = 0.5$ and 1, when d/L smaller than about 0.4.

b/L	0.5		1.0	
d/L	$\kappa_o L$	$\mathcal{F}'(\kappa_o L/2)$	$\kappa_o L$	$\mathcal{F}'(\kappa_o L/2)$
0.1	$4.225 - 2.119i$	$-0.531 + 0.772i$	$2.774 - 2.114i$	$-2.410 + 2.759i$
0.2	$3.124 - 0.869i$	$0.235 + 0.806i$	$2.494 - 1.270i$	$-0.658 + 1.802i$
0.3	$2.505 - 0.493i$	$0.459 + 0.693i$	$2.198 - 0.817i$	$-0.070 + 1.417i$
0.4	$2.111 - 0.319i$	$0.569 + 0.604i$	$1.937 - 0.554i$	$0.220 + 1.195i$
0.5	$1.834 - 0.222i$	$0.634 + 0.535i$	$1.722 - 0.394i$	$0.390 + 1.044i$
0.6	$1.625 - 0.162i$	$0.676 + 0.481i$	$1.547 - 0.291i$	$0.501 + 0.932i$
0.7	$1.462 - 0.123i$	$0.706 + 0.437i$	$1.404 - 0.222i$	$0.579 + 0.845i$
0.8	$1.331 - 0.096i$	$0.729 + 0.401i$	$1.285 - 0.174i$	$0.637 + 0.774i$
0.9	$1.222 - 0.076i$	$0.746 + 0.370i$	$1.184 - 0.138i$	$0.681 + 0.715i$
1.0	$1.130 - 0.061i$	$0.759 + 0.345i$	$1.098 - 0.112i$	$0.715 + 0.665i$
2.0	$0.652 - 0.013i$	$0.815 + 0.204i$	$0.640 - 0.025i$	$0.861 + 0.398i$
3.0	$0.461 - 0.005i$	$0.830 + 0.144i$	$0.455 - 0.009i$	$0.900 + 0.283i$
4.0	$0.356 - 0.002i$	$0.836 + 0.111i$	$0.353 - 0.004i$	$0.917 + 0.219i$
5.0	$0.290 - 0.001i$	$0.840 + 0.092i$	$0.287 - 0.002i$	$0.927 + 0.182i$

Table 1. Rectangular cavity depth mode resonance frequencies for $n = 1$.

2.4 Behaviour near the cavity mouth

The cavity response $\hat{G}_c$ is given exactly by (2.10) when a mass-less piston with normal velocity u_c is inserted in the cavity mouth, separating the interior and exterior flows. For the actual motion we shall assume that the mean normal velocity over the mouth is equal to u_c, and approximate the leading order 'depth mode' response of the cavity by setting

$$\hat{G}_c = u_c \varphi^*(\mathbf{y}), \tag{2.20}$$

where $\partial\varphi^*/\partial y_2 \approx 1$ at $y_2 = 0$ in the cavity mouth except close to the edges of the cavity. The function $\varphi^*(\mathbf{y})$ may be regarded as the exact solution of the Helmholtz equation

representing a source flow at unit mean normal velocity from the mouth of the cavity and satisfying $\partial\varphi^*/\partial y_n = 0$ on S. At large distances from the mouth it represents a rapidly decaying monopole wavefield. In the 'compact limit' in which $\kappa_o L \to 0$, $\varphi^*(\mathbf{y})$ reduces to a solution of Laplace's equation $\nabla^2\varphi^* = 0$, and its local properties for any given cavity can be estimated by the methods of conformal transformation [3].

$\hat{G}_0$ is given by (2.5) in the neighbourhood of $\kappa_o y_2 \sim 0$ just above the cavity. It represents the potential of the incident wave unmodified by the cavity, but can be adjusted so that it also includes the influence of the non-resonant response of the cavity to an aeroacoustic source. This response depends on the unsteady drag on the cavity (parallel to the plane of the wall) and produces a *dipole* contribution to the scattered sound. The adjustment is made correct to an error $\sim O(\kappa_o^2 y_2^2) \ll 1$ simply by replacing $\mathbf{y}$ by $\mathbf{Y}$ in the formula for $\hat{G}_0$ (i.e. by replacing $n_1 y_1 + n_3 y_3$ in the exponential by $n_1 Y_1 + n_3 Y_3 \equiv \mathbf{n}\cdot\mathbf{Y}$) [5]. The modified $\hat{G}_0$ then satisfies $\partial\hat{G}_0/\partial y_n = 0$ on S.

Thus, for $\mathbf{y}$ close to the cavity mouth, and for small or moderate values of $\kappa_o L$, we can write

$$\hat{G}(\mathbf{x},\mathbf{y},\omega) \approx -\frac{\mathrm{e}^{i\kappa_o(|\mathbf{x}|-\mathbf{n}\cdot\mathbf{Y})}}{2\pi|\mathbf{x}|} + u_c\varphi^*(\mathbf{y}), \tag{2.21}$$

where u_c is given by (2.12). By inserting this formula into the integrand of (2.3), we find

$$G(\mathbf{x},\mathbf{y},t-\tau) \approx \frac{1}{2\pi|\mathbf{x}|}\delta\left(t-\tau-\frac{|\mathbf{x}-\mathbf{Y}|}{c_o}+\frac{\mathbf{M}\cdot(\mathbf{X}-\mathbf{Y})}{c_o}\right)$$

$$-\frac{1}{(2\pi)^2 c_o|\mathbf{x}|}\frac{i\,\partial}{\partial t}\int_{-\infty}^{\infty}\varphi^*(\mathbf{y})\frac{\sin(\kappa_o d)\mathcal{S}(\kappa_o L n_1/2)\mathcal{S}(\kappa_o b n_3/2)}{\{\cos(\kappa_o d)-\sin(\kappa_o d)\mathcal{F}(\kappa_o L/2)\}}\,\mathrm{e}^{-i\omega\{t-\tau-|\mathbf{x}|/c_o+\mathbf{M}\cdot(\mathbf{X}-\mathbf{Y})/c_o\}}\,d\omega$$

$$|\mathbf{x}| \to \infty, \tag{2.22}$$

where in the first line we have used the far field approximation $|\mathbf{x}| - \mathbf{n}\cdot\mathbf{Y} \approx |\mathbf{x}-\mathbf{Y}|$ when $|\mathbf{x}| \to \infty$.

The remaining integration in (2.22) can be evaluated by residues, the poles lying in the lower half of the complex ω-plane at the roots of equation (2.15). Let κ_N ($N = 1,\ 2,\ \ldots$) denote the roots (in the lower right half of the complex plane) arranged in order of increasing *positive* real parts – so that κ_1 corresponds to the values given in Table 1 for $b/L = 0.5$ and 1. It is easily seen that to each κ_N there exists a corresponding root with negative real part equal to $-\kappa_N^*$ (where the asterisk denotes complex conjugate). Then

$$G(\mathbf{x},\mathbf{y},t-\tau) \approx \frac{1}{2\pi|\mathbf{x}|}\delta\left(t-\tau-\frac{|\mathbf{x}-\mathbf{Y}|}{c_o}+\frac{\mathbf{M}\cdot(\mathbf{X}-\mathbf{Y})}{c_o}\right)$$

$$+\frac{1}{\pi|\mathbf{x}|}\frac{\partial}{\partial t}\sum_N \mathrm{H}\left(t-\tau-\frac{|\mathbf{x}|}{c_o}+\frac{\mathbf{M}\cdot(\mathbf{X}-\mathbf{Y})}{c_o}\right)$$

$$\times\,\mathcal{R}e\left\{\varphi_N^*(\mathbf{y})\frac{\mathcal{S}(\kappa_N L n_1/2)\mathcal{S}(\kappa_N b n_3/2)\mathrm{e}^{-i\omega_N\{t-\tau-|\mathbf{x}|/c_o+\mathbf{M}\cdot(\mathbf{X}-\mathbf{Y})/c_o\}}}{d\left\{\mathrm{cosec}^2(\kappa_N d)+(L/2d)\mathcal{F}'(\kappa_N L/2)\right\}}\right\}$$

$$|\mathbf{x}|\to\infty, \tag{2.23}$$

where $\omega_N = c_o\kappa_N$ and $\varphi_N^*(\mathbf{y})$ denotes the value of $\varphi^*(\mathbf{y})$ evaluated at $\kappa_o = \kappa_N$.

In practical applications to low Mach number flow only the coherent, large scale resonance represented by the first cavity mode ($N = 1$) will be properly represented by this formula; it can be evaluated using the results given in Table 1.

3. CIRCULAR CYLINDRICAL WALL CAVITY

The representation (2.6) also describes depth modes in the circular cylindrical cavity of Figure 4 in the presence of a rigid, mass-less piston over the cavity mouth. In the exterior region above the cavity [8]

$$\hat{G}_c = -iu_c R \int_0^\infty \frac{\mathrm{J}_0(kr)\mathrm{J}_1(kR)}{\sqrt{\kappa_o^2 - k^2}}\, \mathrm{e}^{iy_2\sqrt{\kappa_o^2-k^2}}\, dk, \quad r = \sqrt{y_1^2 + y_3^2}, \quad y_2 > 0, \tag{3.1}$$

where J_0 and J_1 are Bessel functions [9] and R is the cavity radius.

Similarly, the representation (2.5) of the incident field in the absence of the cavity is unchanged. Then, the analogue of equation (2.12) for u_c becomes

$$u_c = \frac{\kappa_o \sin(\kappa_o d)}{\{\cos(\kappa_o d) - \sin(\kappa_o d)\mathcal{F}(\kappa_o D)\}} \left(\frac{2\mathrm{J}_1(\kappa_o n_{||} R)}{\kappa_o n_{||} R}\right) \frac{\mathrm{e}^{i\kappa_o|\mathbf{x}|}}{2\pi|\mathbf{x}|}, \tag{3.2}$$

where $D = 2R$ is the cavity diameter,

$$\mathcal{F}(\mu) = i\left(1 - \frac{2\mathrm{J}_1(\mu)}{\mu}\right) + \frac{4}{\pi}\int_0^{\frac{\pi}{2}} \sin(\mu\cos\vartheta)\sin^2\vartheta\, d\vartheta, \tag{3.3}$$

and $n_{||} = \sqrt{n_1^2 + n_3^2}$ (c.f. [8] Section 7.4).

As before, the complex resonance frequencies correspond to the roots κ_N ($N = 1,\ 2,\ \ldots$) of

$$\cos(\kappa_o d) - \sin(\kappa_o d)\mathcal{F}(\kappa_o D) = 0.$$

This is solved by numerical integration of equation (2.16), in which we set $z = \kappa_o d$, $X = D/d$, $\mu = zX$, with $\mathcal{F}(\mu)$ defined by (3.3), subject to the initial condition (2.18). Results are presented in Table 2 and Figure 5 for the lowest order depth mode κ_1.

The Green's function for source points $\mathbf{y}$ near the cavity mouth then becomes (c.f. equation (2.22))

$$G(\mathbf{x},\mathbf{y},t-\tau) \approx \frac{1}{2\pi|\mathbf{x}|}\delta\left(t - \tau - \frac{|\mathbf{x}-\mathbf{Y}|}{c_o} + \frac{\mathbf{M}\cdot(\mathbf{X}-\mathbf{Y})}{c_o}\right)$$

$$- \frac{1}{(2\pi)^2 c_o|\mathbf{x}|}\frac{i\partial}{\partial t}\int_{-\infty}^{\infty} \frac{\varphi^*(\mathbf{y})\sin(\kappa_o d)}{\{\cos(\kappa_o d) - \sin(\kappa_o d)\mathcal{F}(\kappa_o D)\}}\left(\frac{2\mathrm{J}_1(\kappa_o n_{||} R)}{\kappa_o n_{||} R}\right) \mathrm{e}^{-i\omega\{t-\tau-|\mathbf{x}|/c_o + \mathbf{M}\cdot(\mathbf{X}-\mathbf{Y})/c_o\}}\, d\omega$$

$$|\mathbf{x}| \to \infty, \tag{3.4}$$

d/D	$\kappa_o D$	$\mathcal{F}'(\kappa_o D)$
0.1	$3.122 - 2.183i$	$-0.828 + 1.143i$
0.2	$2.725 - 1.241i$	$-0.171 + 0.749i$
0.3	$2.351 - 0.770i$	$0.048 + 0.588i$
0.4	$2.045 - 0.511i$	$0.156 + 0.494i$
0.5	$1.803 - 0.358i$	$0.219 + 0.431i$
0.6	$1.611 - 0.262i$	$0.260 + 0.383i$
0.7	$1.456 - 0.198i$	$0.289 + 0.346i$
0.8	$1.328 - 0.153i$	$0.311 + 0.317i$
0.9	$1.221 - 0.121i$	$0.327 + 0.292i$
1.0	$1.130 - 0.098i$	$0.340 + 0.271i$
2.0	$0.652 - 0.021i$	$0.394 + 0.160i$
3.0	$0.456 - 0.009i$	$0.408 + 0.112i$
4.0	$0.355 - 0.003i$	$0.415 + 0.088i$
5.0	$0.297 - 0.000i$	$0.419 + 0.074i$

Table 2. Circular cylindrical cavity depth mode resonance frequencies for $n = 1$.

and similarly, by residues,

$$
\begin{aligned}
G(\mathbf{x},\mathbf{y},t-\tau) \;\approx\; & \frac{1}{2\pi|\mathbf{x}|}\delta\left(t-\tau-\frac{|\mathbf{x}-\mathbf{Y}|}{c_o}+\frac{\mathbf{M}\cdot(\mathbf{X}-\mathbf{Y})}{c_o}\right) \\
& + \frac{1}{\pi|\mathbf{x}|}\frac{\partial}{\partial t}\sum_N \mathrm{H}\left(t-\tau-\frac{|\mathbf{x}|}{c_o}+\frac{\mathbf{M}\cdot(\mathbf{X}-\mathbf{Y})}{c_o}\right) \\
& \times \mathcal{R}e\left\{\left(\frac{2\mathrm{J}_1(\kappa_N n_{||} R)}{\kappa_N n_{||} R}\right)\frac{\varphi_N^*(\mathbf{y})\mathrm{e}^{-i\omega_N\{t-\tau-|\mathbf{x}|/c_o+\mathbf{M}\cdot(\mathbf{X}-\mathbf{Y})/c_o\}}}{d\left\{\mathrm{cosec}^2(\kappa_N d)+(D/d)\mathcal{F}'(\kappa_N D)\right\}}\right\} \\
& \qquad\qquad |\mathbf{x}| \to \infty, \qquad\qquad (3.5)
\end{aligned}
$$

where $\omega_N = c_o\kappa_N$, $\varphi_N^*(\mathbf{y})$ denotes the value of $\varphi^*(\mathbf{y})$ evaluated at $\kappa_o = \kappa_N$, and for $N = 1$ the value of $\mathcal{F}'(\kappa_1 D)$ is given in Table 2.

4. EXCITATION OF CAVITY RESONANCES BY VORTEX SHEDDING

4.1 Aerodynamically generated sound

To illustrate the application of these Green's functions to study flow excited cavity oscillations we shall consider the generalized configurations depicted schematically in Figure 6, of low Mach number, nominally steady flow in the x_1-direction past a rectangular wall cavity in the presence of a fixed, bluff body in the main stream adjacent to the cavity mouth. Of particular practical importance are spanwise-orientated cylindrical cross-beams: Figures 6a and 6b show cases where a cross-beam in the form of a circular cylinder is respectively situated centrally above the cavity mouth and just upstream of the leading edge of the cavity. Vortex shedding from this beam can be expected to excite the cavity resonance.

The acoustic pressure $p(\mathbf{x},t)$ at the far field point $\mathbf{x}$ at time t in fluid of mean density ρ_o is given in terms of the flow velocity $\mathbf{v}(\mathbf{x},t)$ and the vorticity $\boldsymbol{\omega}(\mathbf{x},t) = \operatorname{curl}\mathbf{v}$ in the vicinity of the cavity by [2, 5]

$$p \approx \frac{-\rho_o}{(1+M\cos\theta)} \int (\boldsymbol{\omega}\wedge\mathbf{v})(\mathbf{y},\tau)\cdot\frac{\partial G}{\partial \mathbf{y}}(\mathbf{x},\mathbf{y},t-\tau)\,d^3\mathbf{y}d\tau, \quad |\mathbf{x}|\to\infty, \tag{4.1}$$

where the integration is over all values of the retarded time τ and the fluid region where the vorticity $\boldsymbol{\omega}\neq\mathbf{0}$, and θ is the angle between the observer direction and the mean stream, so that $\cos\theta \equiv n_1$.

The Green's function in (4.1) must have vanishing normal derivative on all fixed surfaces in the flow. It can therefore be taken in the form (2.22) or (2.23) when the cross-beam is absent. Analytical details for a simplified model of this case were discussed in [2], where it was confirmed that the principal source of cavity noise was related to the unsteady drag experienced by the cavity, produced by pressure fluctuations on the back wall near the trailing edge (A in Figure 6a). The drag fluctuations generate both 'non-resonant' dipole sound, associated with the first, δ-function term on the right of (2.22), and monopole sound, corresponding to the excitation of the lowest order cavity resonance and accounted for by the second term in (2.22).

4.2 Vortex shedding from an adjacent bluff body

The more general cases shown in Figure 6, involving the cross-beam can be treated by simple extension of the Green's function (2.22), provided the cross-sectional area of the

beam is small. To fix ideas consider a beam of circular cross-section of radius $R_o \ll L$. In case (a) (Figure 6a), where the beam is above the mouth of the cavity, with its axis along $x_1 = 0,\ x_2 = h$, say, the functions $\varphi^*(\mathbf{y})$ and $\mathbf{Y}(\mathbf{y})$ of (2.22) are given in the neighbourhood of the beam by

$$\varphi^* \approx y_2, \quad Y_1 \approx y_1, \quad Y_3 \approx y_3. \tag{4.2}$$

When $\kappa_o R_o \ll 1$ the local behaviour of the Green's function in the immediate vicinity of the cross-beam is the same as when the fluid is treated as incompressible. We can therefore extend the validity of (2.22) and (2.23) to include the influence of the beam by augmenting the local approximations (4.2) by solutions of Laplace's equation that are negligible at distances $\gg R_o$ from the beam, but which just ensure that $\partial G/\partial y_n = 0$ on the surface of the beam. For a circular cylindrical beam this is equivalent to replacing φ^* and $\mathbf{Y} \equiv (Y_1, 0, Y_3)$ respectively by Φ^* and $\boldsymbol{\mathcal{Y}} \equiv (\mathcal{Y}_1, 0, \mathcal{Y}_3)$, where

$$\left.\begin{aligned} \Phi^*(\mathbf{y}) &= \varphi^*(\mathbf{y}) + \frac{(y_2-h)R_o^2}{y_1^2+(y_2-h)^2} \\ \mathcal{Y}_1(\mathbf{y}) &= Y_1(\mathbf{y}) + \frac{y_1 R_o^2}{y_1^2+(y_2-h)^2}, \quad \mathcal{Y}_3 = Y_3(\mathbf{y}) \end{aligned}\right\} \tag{4.3}$$

The sound produced by the resonant response of the cavity to vortex shedding from the beam can now be obtained from (4.1) by substituting for G the second term on the right of (2.22) in which φ^* is replaced by Φ^*. The result can be written

$$\begin{aligned} p \;\approx\; & \frac{1}{(2\pi)^2 c_o(1+M\cos\theta)|\mathbf{x}|}\frac{i\partial}{\partial t}\int_{-\infty}^{\infty} F(\tau)\frac{\sin(\kappa_o d)\mathcal{S}(\kappa_o L n_1/2)\mathcal{S}(\kappa_o b n_3/2)}{\{\cos(\kappa_o d)-\sin(\kappa_o d)\mathcal{F}(\kappa_o L/2)\}} \\ & \qquad \times \mathrm{e}^{-i\omega\{t-\tau-|\mathbf{x}|(1-M\cos\theta)/c_o\}}\, d\omega\, d\tau, \end{aligned} \tag{4.4}$$

$$\begin{aligned} = \; & \frac{1}{2\pi(1+M\cos\theta)|\mathbf{x}|}\int_{-\infty}^{\infty} \hat{F}(\omega)\frac{\kappa_o \sin(\kappa_o d)\mathcal{S}(\kappa_o L n_1/2)\mathcal{S}(\kappa_o b n_3/2)}{\{\cos(\kappa_o d)-\sin(\kappa_o d)\mathcal{F}(\kappa_o L/2)\}} \\ & \qquad \times \mathrm{e}^{-i\omega\{t-|\mathbf{x}|(1-M\cos\theta)/c_o\}}\, d\omega, \quad |\mathbf{x}| \to \infty, \end{aligned} \tag{4.5}$$

where

$$F(\tau) = \rho_o \int (\boldsymbol{\omega}\wedge\mathbf{v})(\mathbf{y},\tau)\cdot\frac{\partial\Phi^*}{\partial\mathbf{y}}(\mathbf{y})\, d^3\mathbf{y}, \quad \text{and} \quad \hat{F}(\omega) = \frac{1}{2\pi}\int_{-\infty}^{\infty} F(\tau)\mathrm{e}^{i\omega\tau}\, d\tau. \tag{4.6}$$

In equations (4.4) and (4.5) we have neglected a contribution to $\partial G/\partial\mathbf{y}$ from the term $\mathbf{M}\cdot\mathbf{Y}(\mathbf{y})$ in the argument of the exponential in (2.22). It is easily verified that the contribution from this term is $O(M\kappa_o h) \ll 1$ smaller than the contribution from $\partial\Phi^*/\partial\mathbf{y}$.

In these results $\Phi^*(\mathbf{y})$ represents in the vicinity of the beam the velocity potential of an irrotational flow past the beam having unit speed in the x_2-direction at distances $\gg R_o$ from the beam, and the first formula in (4.6) is therefore identical with that determining the unsteady force on the beam in the x_2-direction produced by the hydrodynamic flow near the beam (in particular by vortex shedding from the beam) [2, 5]. Hence, the contribution from the beam to cavity mode-excitation is produced by the fluctuating *lift force* $F(t)$ on the beam.

This, conclusion, however, is correct only for a beam placed above the mid-section of the cavity mouth. In the case illustrated in Figure 6b, where the beam is just upstream of the leading edge of the cavity (or equivalently, just downstream of the trailing edge), the function $\varphi^*(\mathbf{y})$ is the velocity potential of a flow that is essentially *parallel* to the wall in the neighbourhood of the beam. The modified potential $\Phi^*(\mathbf{y})$ must therefore represent a flow past the beam parallel to the wall; the function $F(\tau)$ defined by the first integral in (4.6) is then proportional to the force on the beam in the x_1-direction [5], so that the radiation by cavity resonances is now associated with the *drag* fluctuations on the beam. For other locations of the beam, between the edges of the cavity and above the mid-section, the direction of the net force on the beam responsible for the cavity oscillations will be inclined to both the mean flow and wall normal directions.

4.3 Efficiency of cavity resonance generation

Let $\Phi(\omega, \mathbf{x})$ denote the acoustic far field frequency spectrum, defined such that

$$\langle p^2(\mathbf{x}, t)\rangle = \int_0^\infty \Phi(\omega, \mathbf{x})\, d\omega, \tag{4.7}$$

where the angle brackets $\langle\ \rangle$ denote an ensemble average. If the unsteady exciting force $F(t)$ on the beam is stationary random in time, with frequency spectrum $\Phi_{FF}(\omega)$, then

$$\langle \hat{F}(\omega)\hat{F}^*(\omega')\rangle = \delta(\omega - \omega')\Phi_{FF}(\omega).$$

It follows that when the cavity resonance can be assumed to dominate the radiation,

$$\Phi(\omega, \mathbf{x}) \approx \frac{\Phi_{FF}(\omega)}{2\pi^2(1 + M\cos\theta)^2(|\mathbf{x}|d)^2}\mathcal{S}^2\left(\frac{\kappa_o L n_1}{2}\right)\mathcal{S}^2\left(\frac{\kappa_o b n_3}{2}\right)\Psi(\kappa_o L), \quad |\mathbf{x}| \to \infty, \tag{4.8}$$

where

$$\Psi(\kappa_o L) = \frac{(\kappa_o d)^2 \sin^2(\kappa_o d)}{|\cos(\kappa_o d) - \sin(\kappa_o d)\mathcal{F}(\kappa_o L/2)|^2}. \tag{4.9}$$

In equation (4.8) the functions $\mathcal{S}(\kappa_o L n_1/2)$, $\mathcal{S}(\kappa_o b n_3/2)$ determine the *directivity* of the sound. They are equal to 1 at low frequencies in all directions $\mathbf{n} = \mathbf{x}/|\mathbf{x}|$, when the radiation is essentially omnidirectional, but become progressively peaked in directions normal to the wall when $\kappa_o L \gg 1$ (see [8] for graphical illustrations). The function $\Psi(\kappa_o L)$ governs the efficiency with which the cavity resonance is excited. No resonances can be excited at very low frequencies ($\kappa_o d \to 0$), when $\Psi(\kappa_o L) \sim (\kappa_o d)^4$. In this limit the acoustic wavelength greatly exceeds the cavity depth and the amplitude of the cavity induced sound is the same as that of a relatively weak Lighthill quadrupole source [5, 10]. The force spectrum $\Phi_{FF}(\omega)$ is expected to be large when the Strouhal number $fR_o/U \sim 0.1$ ($f = \omega/2\pi$), and the cavity resonance will therefore tend to be preferentially excited for an appropriately large mean flow velocity U, when this value of the Strouhal number corresponds to a frequency where $\Psi(\kappa_o L)$ is large. This occurs where the denominator in (4.9) is small. But, we have seen that the zeros of the denominator lie progressively far into the lower complex plane as the depth ratio d/L decreases, corresponding to increased radiation damping of the resonance. This is illustrated in Figure 7, which depicts the variation of $\Psi(\kappa_o L)$ for a square cavity ($b = L$) for real values of κ_o in the range where the first cavity mode might be expected to be excited. The real resonance frequencies can be approximately identified with the real parts of the frequencies given in Table 1 (or indicated by the large dots in Figure 3). Figure 7 shows that a significant resonance peak occurs in $\Psi(\kappa_o L)$ only when d/L exceeds about 0.4. For smaller values of d/L, for very shallow cavities, the radiation damping is so large that a genuine resonance peak does not exist. When $d/L > 0.6$, however, the resonances become firmly established and excitation at the resonance frequency can be expected to supply a strong tonal contribution to the radiation field (the difference in peak levels between $d/L = 1$ and $d/L = 0.6$ is about 7dB, and about 12 dB between $d/L = 1$ and 0.4).

5. CONCLUSION

The acoustic radiation produced by nominally steady, low Mach number flow over a wall cavity has two principal components. The unsteady drag produced by vortex-generated pressure fluctuations applied to the trailing cavity wall is a source of 'dipole sound', which radiates preferentially in directions parallel to the mean stream. These drag fluctuations can also excite volumetric fluctuations of fluid within the cavity, thereby contributing a monopole component of the sound. The unsteady lift and drag forces experienced by a bluff body adjacent to the cavity can also excite the cavity monopole. The unsteady lift (normal to the wall) is the dominant source when the body is located centrally above the mouth of the cavity; the contribution from the drag becomes significant when the body is close to the leading or trailing edge of the cavity, and becomes the principal cavity-mode source when the body is near the wall just upstream or downstream of the cavity.

The Green's functions given in this chapter can be used to make quantitative predictions of the sound for rectangular and circular cylindrical cavities from a knowledge of the hydrodynamic flow in the vicinity of the cavity. At low Mach numbers the sound will be a 'small by-product' of the hydrodynamic motions having a negligible back-reaction on the main flow, whose properties can therefore be derived from observation or from calculation based on an incompressible approximation to the Navier-Stokes equations. Only the low frequency cavity resonances are expected to be excited at low Mach numbers. The resonance frequencies are complex, the imaginary part representing dissipation associated primarily with radiation damping in the case of a shallow, open cavity. The damping can significantly modify the nature of the volumetric response of the cavity, completely eliminating from the acoustic spectrum the presence of a distinct resonance peak. Our numerical results for a cavity with a square mouth indicate that such peaks are likely to be present in the acoustic spectrum only when the cavity depth d exceeds about half the cavity length L. The strong radiation damping experienced by a cavity when d/L is small makes it impossible for the cavity to store significant resonant energy; volumetric pulsations of fluid within the cavity then represent a driven response due to broad-band external forcing by the unsteady flow. For a very shallow cavity the efficiency of the sound generated by this forced motion is comparable to that produced by a free field turbulence quadrupole, and is therefore negligible at low Mach numbers when compared to the dipole sound generated by the cavity drag.

In practice, of course, the absence of a cavity resonance contribution to the far field

sound does not preclude strong tonal radiation from the cavity. The resonances in this case are governed *not* by the cavity volumetric dimensions but by the streamwise length of the cavity, which determines the 'Rossiter frequencies' [5, 11 - 13] associated with hydrodynamic oscillations involving vortex-edge interactions at the trailing edge whose feedback to the leading edge amplifies the production of shear layer vorticity at certain preferred frequencies. Very intense tonal radiation would be expected when the mean flow conditions cause the cavity resonance frequency and a Rossiter frequency to coincide.

REFERENCES

1. M. S. Howe 1997 Edge, cavity and aperture tones at very low Mach numbers. *Journal of Fluid Mechanics* **330**, 61 - 84.
2. M. S. Howe 2002 Mechanism of sound generation by low Mach number flow over a wall cavity. Chapter 1 and *Journal of Sound and Vibration* (in press).
3. G. K. Batchelor 1967 *An Introduction to Fluid Dynamics,* Cambridge University Press.
4. K. Taylor 1978 A transformation of the acoustic equation with implications for wind tunnel and low speed flight tests. *Proceedings of the Royal Society of London* **A363**, 271 - 281.
5. M. S. Howe 1998 *Acoustics of fluid-structure interactions,* Cambridge University Press.
6. A. Powell 1961 On the edgetone. *Journal of the Acoustical Society of America* **33**, 395 - 409.
7. Lord Rayleigh 1945 *Theory of Sound,* Volume 2. New York: Dover.
8. P. M. Morse and K. U. Ingard 1968 *Theoretical Acoustics.* New York: McGraw-Hill.
9. M. Abramowitz and I. A. Stegun (editors) 1970 *Handbook of Mathematical Functions* (Ninth corrected printing), US Department of Commerce, National Bureau of Standards Applied Mathematics Series No.55.
10. M. J. Lighthill 1952 On sound generated aerodynamically. Part I: General theory. *Proceedings of the Royal Society of London* **A211**, 564 - 587.
11. J. E. Rossiter 1962 The effect of cavities on the buffeting of aircraft. *Royal Aircraft Establishment Tech. Memo.* 754.
12. D. Rockwell 1983 Oscillations of impinging shear layers. *American Institute of Aeronautics and Astronautics Journal* **21**, 645 - 664.
13. D. Rockwell and E. Naudascher 1978 Review - self-sustaining oscillation of flow past cavities. *Transactions of the American Society of Mechanical Engineers, Journal of Fluids Engineering* **100**, 152 - 165.

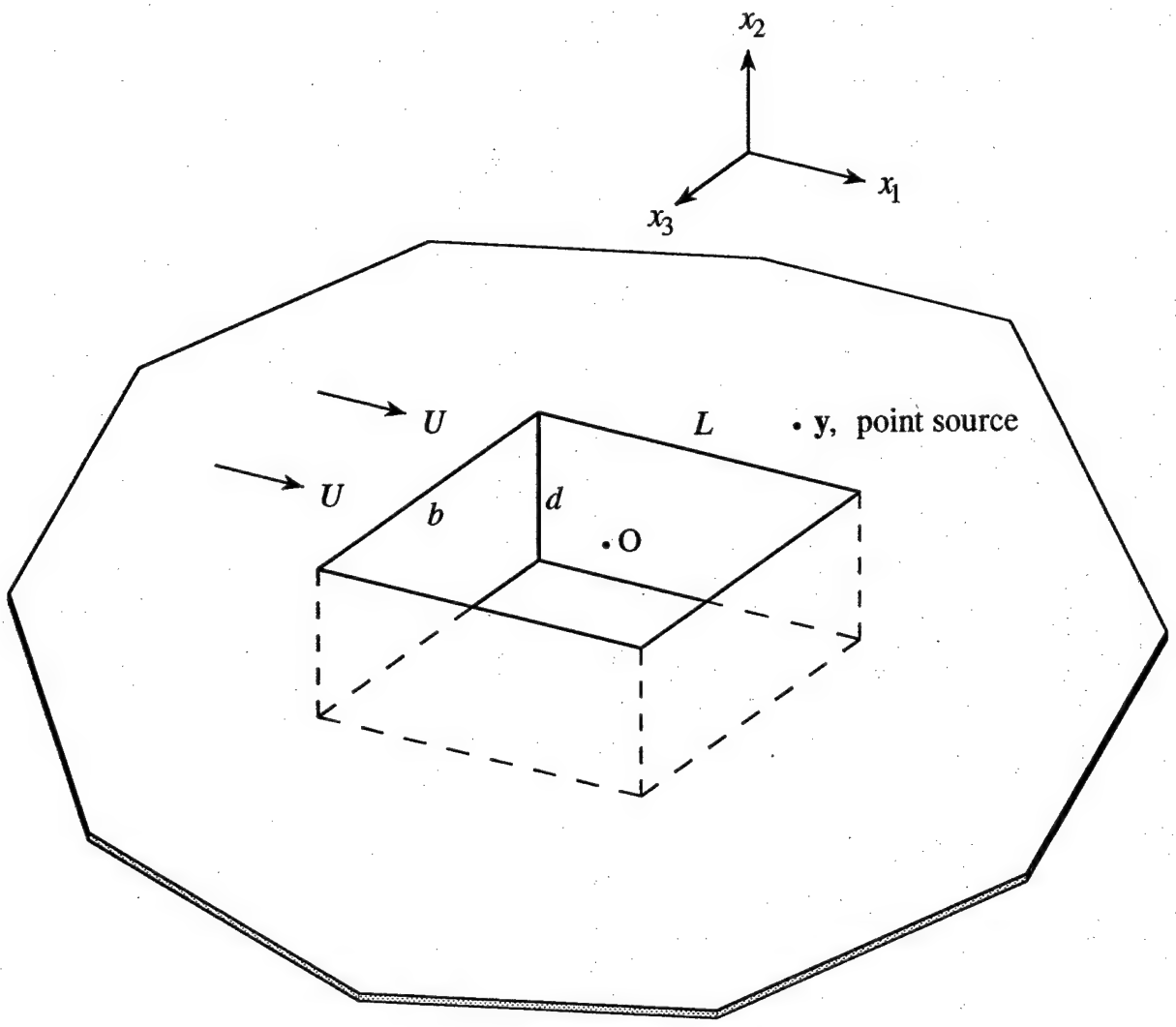

Figure 1. Point source at **y** adjacent to a rectangular wall cavity of depth d and streamwise length L in the presence of low Mach number steady flow at speed U in the x_1-direction.

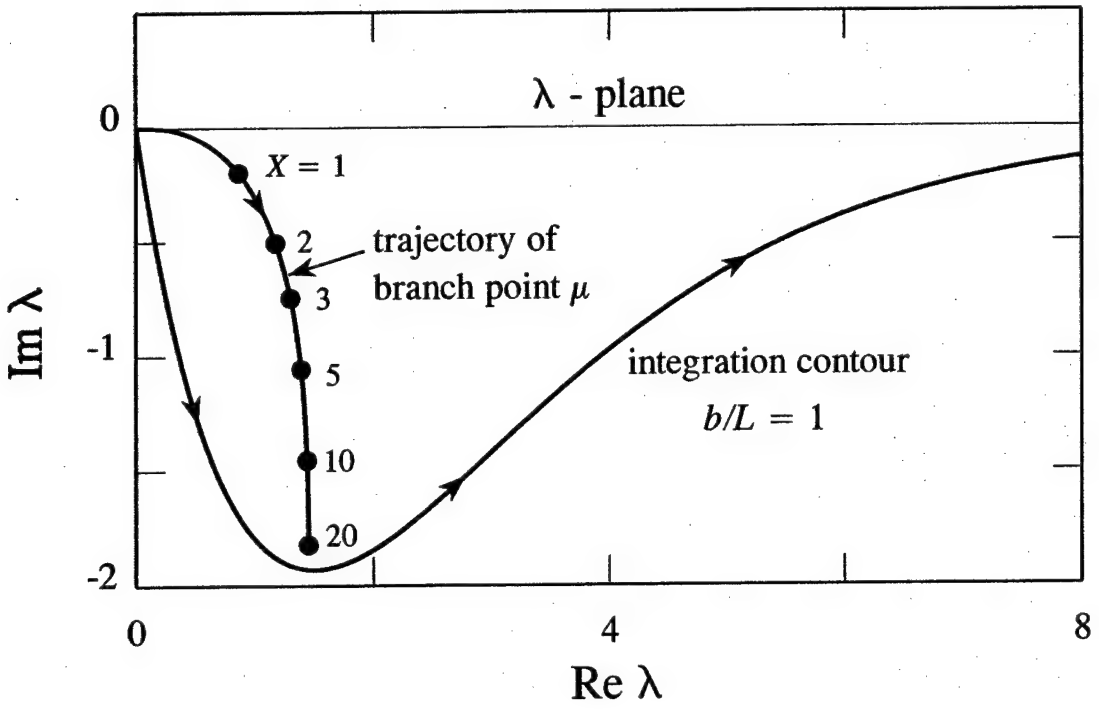

Figure 2. Trajectory in the complex λ-plane of the branch point at $\lambda = \mu(X)$ of $\sqrt{\mu^2 - \lambda^2}$ for $n = 1$ and $b/L = 1$ when X increases over the interval $0 < X < 20$; the integration paths in (2.15) and (2.17) must be displaced from the real axis onto the contour (2.18) passing below the branch point.

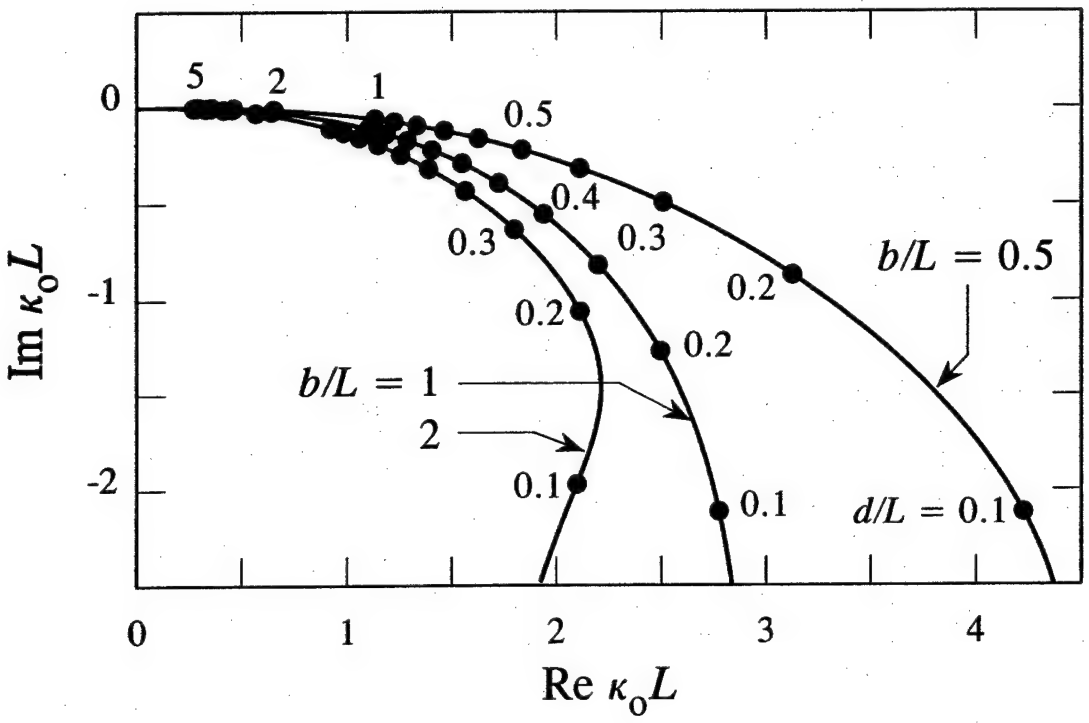

Figure 3. Rectangular cavity complex resonance frequency $\kappa_o L$ for the lowest order depth mode $n = 1$ when the cavity aspect ratio $\alpha \equiv b/L = 0.5,\ 1,\ 2..$

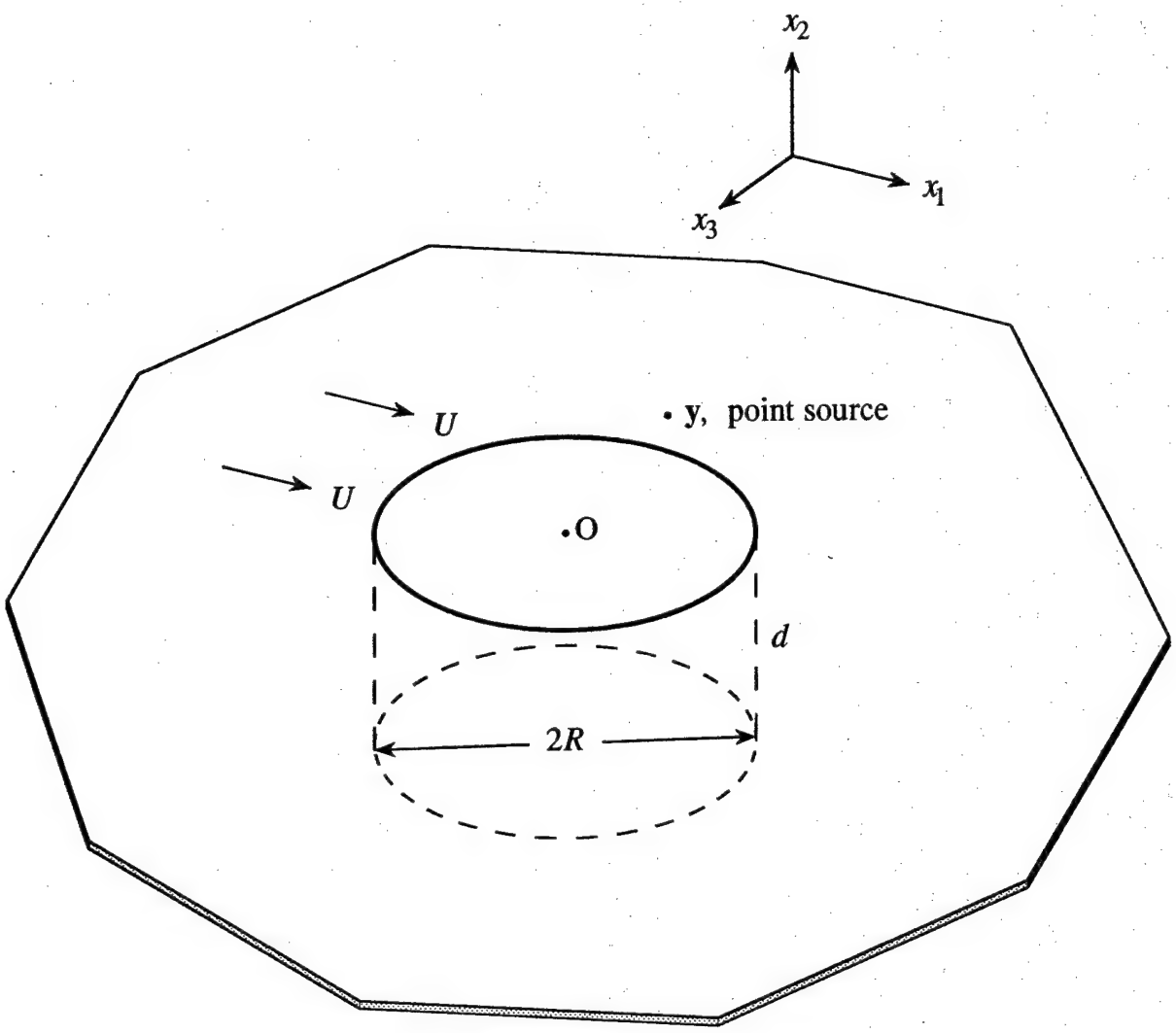

Figure 4. Point source at **y** adjacent to a circular cylindrical wall cavity of depth d and radius R in the presence of low Mach number steady flow at speed U in the x_1-direction.

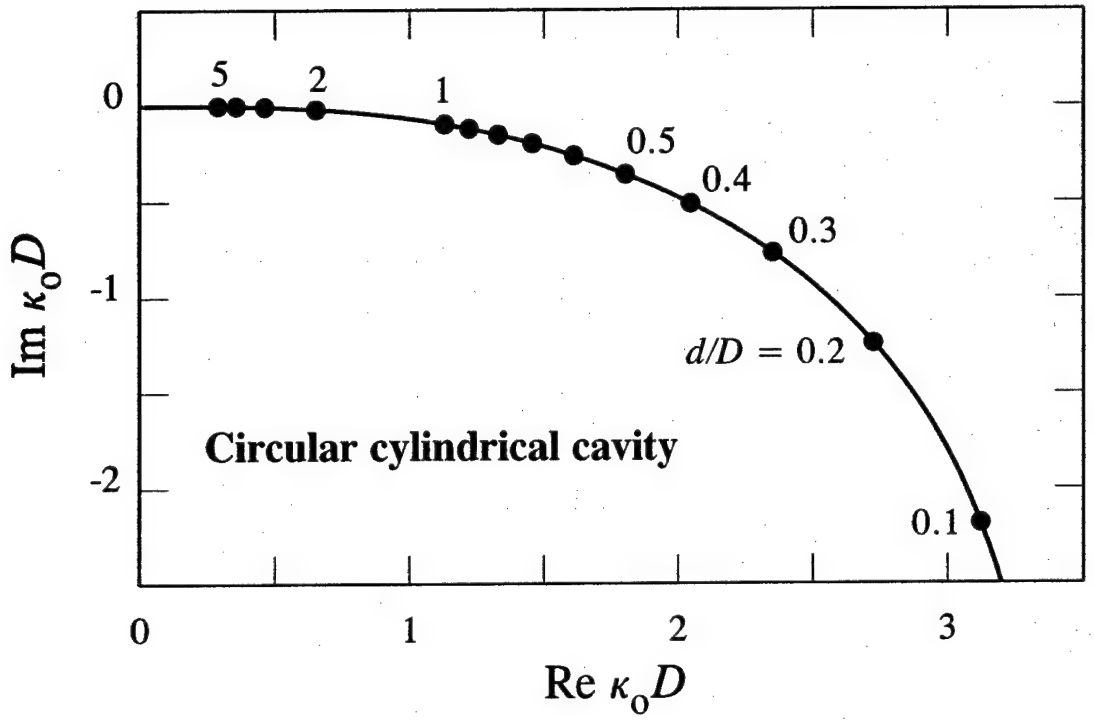

Figure 5. Complex resonance frequency $\kappa_o D$ of the lowest order depth mode $n = 1$ for a circular cylindrical cavity of diameter D and depth d.

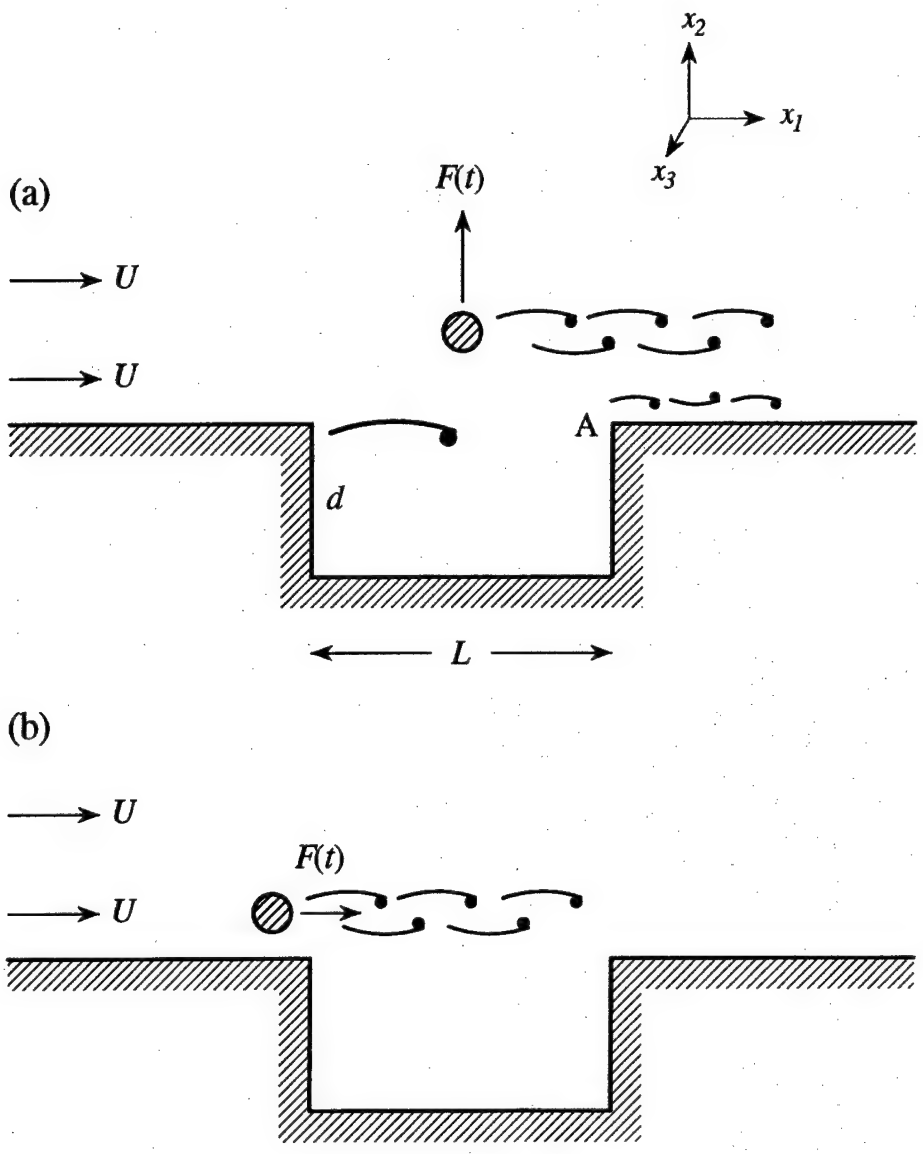

Figure 6. Excitation of cavity resonance:
(a) unsteady lift fluctuations $F(t)$ on an adjacent, centrally located bluff body, and unsteady drag produced by vorticity near the cavity trailing edge A;
(b) unsteady drag $F(t)$ on an adjacent body just upstream of the cavity.

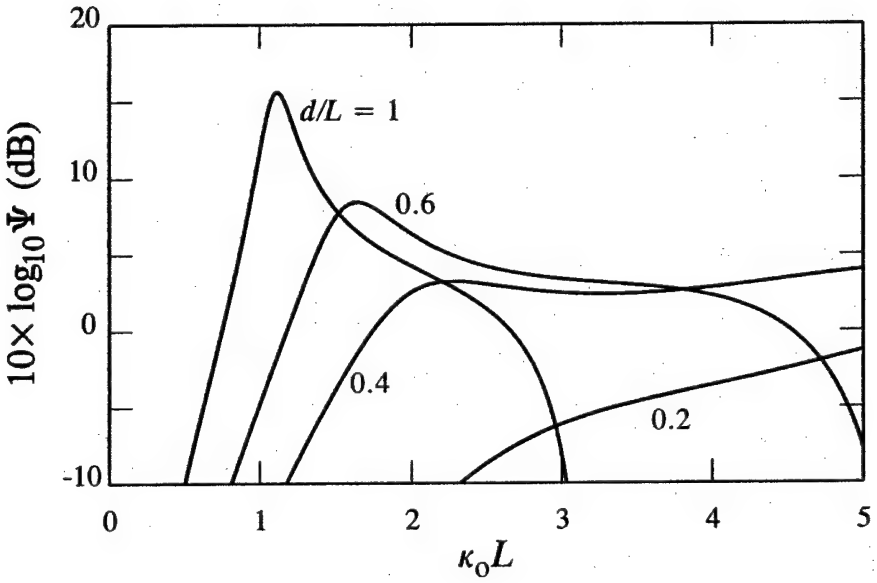

Figure 7. The efficiency of excitation of the lowest order resonance is governed by

$$\Psi(\kappa_o L) = \frac{(\kappa_o d)^2 \sin^2(\kappa_o d)}{|\cos(\kappa_o d) - \sin(\kappa_o d)\mathcal{F}(\kappa_o L/2)|^2},$$

whose variation with frequency is shown for a square cavity ($b = L$) for $d/L = 0.2,\ 0.4,\ 0.6,\ 1.0$. (The curve for $d/L = 1$ is shown only in the interval $0 < \kappa_o L < 3$ containing the peak of the first resonance.)

CHAPTER 3

CAVITY MODE EXCITATION BY VORTEX SHEDDING FROM A CROSS-BEAM

SUMMARY

An analysis is made of the tonal acoustic radiation produced by nominally steady, low Mach number flow past a shallow, rectangular wall cavity in the presence of a cross-beam in the flow adjacent to the cavity. At 'lock-on' the frequency of vortex shedding from the beam is equal to one of the resonant frequencies of the cavity. The sound produced by this vorticity is augmented by the presence of the cavity and is calculated for the lowest order resonance frequency of the cavity by using a Green's function derived by Howe (*International Journal of Aeroacoustics* **2**, 347 - 365, 2003). Except for beams of very small cross-section, the efficiency of the aeroacoustic coupling between the beam and the cavity depends on the position of the beam above the cavity. Our results indicate that the coupling is strongest when the beam lies above the cavity mouth between the cavity leading edge and the centre of the mouth. The analysis makes use of two alternative models of vortex shedding, involving an either array of discrete, rectilinear vortices or a continuous, time-harmonic vortex sheet in the wake of the beam. At lock-on each of these models supplies essentially identical predictions of the acoustic sound power radiated directly away from the cavity.

1. INTRODUCTION

The generation of sound by a nominally uniform, irrotational mean flow usually occurs via mechanisms involving the production of vorticity [1]. In the particular case of steady flow at low Mach number past a shallow wall cavity the sound is associated with monopole and dipole sources (see [2, 3] and references cited therein). The dipole dominates the radiation at very low Mach numbers $M \ll 0.1$, say, and is the most important source, for example, in underwater flow ($M \sim 0.01$) past a cavity with 'hydraulically rigid' walls (so that monopole sources generated by flexing of the cavity walls are absent). The dipole is aligned with the mean flow direction and is equal in strength to the fluctuating cavity drag produced by vortex shedding; its radiation field peaks in directions upstream and downstream of the cavity. At higher Mach numbers ($M \sim 0.1$) shed vorticity excites the low order cavity depth (or 'Helmholtz') mode, which is equivalent to a monopole source of sound whose amplitude can greatly exceed that of the dipole at frequencies close to resonance. Very recent numerical studies of monopole excitation are discussed by Mallick *et al.* [5].

When the vorticity field and its motion are known the acoustic pressure $p(\mathbf{x}, t)$ at position $\mathbf{x}$ and time t can readily be calculated for low Mach number, high Reynolds number flow from the vortex sound equation [1]

$$p(\mathbf{x}, t) \approx -\rho_o \int (\boldsymbol{\omega} \wedge \mathbf{v})(\mathbf{y}, \tau) \cdot \frac{\partial G}{\partial \mathbf{y}}(\mathbf{x}, \mathbf{y}, t - \tau)\, d^3\mathbf{y} d\tau. \tag{1}$$

In this formula $\mathbf{v}$ and $\boldsymbol{\omega} = \operatorname{curl} \mathbf{v}$ are respectively the fluid velocity and vorticity, ρ_o is the mean density (assumed uniform), and $G(\mathbf{x}, \mathbf{y}, t - \tau)$ is the appropriate aeroacoustic Green's function; for a rigid wall and rigid cavity interior surfaces G is required to have vanishing normal surface derivatives. The integrations in (1) are over all values of the retarded time τ and over the fluid region where the vorticity $\boldsymbol{\omega} \neq \mathbf{0}$.

An approximate formula for $G(\mathbf{x}, \mathbf{y}, t - \tau)$ was derived in [4] for radiation from a shallow, rigid rectangular cavity orientated with respect to the mean flow and coordinate axes as in Figure 1. The cavity has depth d and sides of lengths L and b respectively in the streamwise and spanwise directions, and the approximation was valid at sufficiently small Mach number that the principal resonant oscillations of the cavity could be identified with 'depth' modes, producing essentially coherent reciprocating flow across the mouth of the cavity. It was also shown in [4] how the utility of the Green's function could be extended to cover the case illustrated in profile in Figure 2, where a spanwise, rigid cross-beam is present in the flow adjacent to the cavity.

Vortex shedding from this beam can be strongly coupled to resonant oscillations excited in the cavity [6 - 9]. In Figure 3 the axis of the cross-beam lies along the line $x_1 = x_c,\ x_2 = y_c$, where the origin of coordinates $\mathbf{x} = (x_1, x_2, x_3)$ (with corresponding unit vectors $\mathbf{i}, \mathbf{j}, \mathbf{k}$) is taken at O in the plane of the wall at the centroid of the cavity mouth, with the x_2-axis normal to the wall and directed into the fluid, as in Figure 1. In the simple case when the cross-section of the beam is a square of side ℓ, strong coupling to the cavity occurs when the Strouhal number $f\ell/U \sim 0.2$ where f is a cavity resonance frequency and U is the mean flow velocity past the beam [1, 9]. In these circumstances vortex shedding from the beam and the resonant response of the cavity are locked together in a nonlinear fashion that results in relatively large amplitude radiation at or very near the resonance frequency. In this chapter we shall examine a simple model of vortex shedding from the beam in order to estimate how the efficiency of cavity mode excitation at 'lock-on' varies with the stream wise position of the beam, whether centrally located as in Figure 2, or located at positions near the leading and trailing edges.

To do this we shall make use of the Green's function derived in [4] together with associated numerical predictions of the *complex* cavity resonance frequencies, where the imaginary part of the frequency accounts for the decay of a cavity mode as a result of radiation damping, which is large for shallow cavities. The formal solution of the aeroacoustic problem is discussed in detail in Section 2, where the vortex wake of the cross-beam is modelled by a sequence of discrete, rectilinear vortices. Numerical results are presented (Section 3) for a cavity with a square mouth for several positions of the cross-beam. In Section 4 analogous predictions are briefly discussed for a continuous wake modelled by a time-harmonic vortex sheet.

2. FORMULATION

Figure 3 depicts the general configuration of the beam and cavity, and the first of two simplified models of vortex shedding to be examined. It will be assumed that at resonance lock-on vortex shedding from the beam occurs periodically, and in the first instance the shed vorticity will be modelled by a sequence of equally spaced line vortices (parallel to the spanwise, x_3 coordinate axis) of alternating strengths $\pm\Gamma$ and infinitesimal core radii. The vortices convect in the streamwise direction at constant speed U_c along a common path in the plane $x_2 = y_c$; this is equivalent to assuming that the vortices are released into the flow along the line $x_1 = x_r \equiv x_c + \ell/2,\ x_2 = y_c$ spanning the rear face of the beam, as indicated in Figure 3. The principal dynamic effect of shedding is to cause fluctuations in the lift and drag on the beam [1, 4]; only minor details of the time dependence of these fluctuations are affected by the location of the point of separation.

2.1 The acoustic pressure

Let the nth vortex be released at time $t_n \equiv n\tau_o$. The period of the whole motion is $2\tau_o$, with fundamental frequency $f_o = 1/2\tau_o$, and the vorticity $\boldsymbol{\omega}_n$ of the nth vortex can be written

$$\boldsymbol{\omega}_n = (-1)^n \Gamma \mathbf{k}\, \delta\big(x_1 - x_r - U_c(t - t_n)\big)\delta(x_2 - y_c)\mathrm{H}(t - t_n), \quad x_r = x_c + \frac{\ell}{2}, \tag{2}$$

where H is the Heaviside step function. The velocity at the core of the vortex is $\mathbf{v} = U_c\mathbf{i}$. Therefore $\boldsymbol{\omega}_n \wedge \mathbf{v} = \omega_n U_c \mathbf{j}$, and the acoustic pressure p_n, say, attributable to the nth vortex is given from equation (1) by

$$p_n(\mathbf{x}, t) \approx -(-1)^n \rho_o \Gamma U_c \iint_{-\infty}^{\infty} \mathrm{H}(\tau - t_n) \frac{\partial G}{\partial y_2}\big(\mathbf{x}, x_r + U_c(\tau - t_n), y_c, y_3, t - \tau\big)\, dy_3 d\tau. \tag{3}$$

This integral will be evaluated to determine the monopole component of the sound radiated from the cavity at lock-on. This would be essentially omnidirectional at very low frequencies, but at the moderate frequencies that characterise the lowest order cavity depth mode it can actually exhibit a small dependence on direction that is of no significance for the present discussion (see [4]). It will therefore be sufficient to calculate the monopole sound only in radiation directions *normal* to the wall. This is done by retaining the following component of the low Mach number approximation for G (from [4], equation (2.23))

$$G(\mathbf{x}, \mathbf{y}, t - \tau) \approx \frac{\varphi^*(\mathbf{y})}{\pi |\mathbf{x}| \mathcal{L}} \frac{\partial}{\partial t} \left(\mathrm{H}\left([t] - \tau\right) \cos\{\Omega([t] - \tau) + \alpha\} \mathrm{e}^{-\epsilon([t]-\tau)}\right), \quad |\mathbf{x}| \to \infty, \tag{4}$$

where $[t] = t - |\mathbf{x}|/c_o$ is the retarded time, and c_o is the mean sound speed. The function $\varphi^*(\mathbf{x})$ (which has the dimensions of length) is that solution of Laplace's equation that represents the incompressible potential flow from the mouth of the cavity *in the presence of the beam* that would be produced by motion of the base of the cavity at unit speed in the positive x_2 direction.

The approximation (4) represents the response of the cavity at its lowest complex resonance (radian) frequency

$$\omega = \Omega - i\epsilon, \tag{5}$$

values of which are tabulated in [4] for a range of values of d/L and for $b/L = 0.5,\ 1$. The length $\mathcal{L}$ (> 0) and phase angle α are defined by

$$\mathcal{L}\mathrm{e}^{i\alpha} = d\left[\mathrm{cosec}^2\left(\frac{\omega d}{c_o}\right) + \frac{L}{2d}\mathcal{F}'\left(\frac{\omega L}{2c_o}\right)\right] \tag{6}$$

where the complex valued function $\mathcal{F}'$ is also tabulated in [4].

The integration in equation (3) with respect to y_3 is taken over the spanwise extent of the vortex. However, just above the wall the function $\partial\varphi^*/\partial y_2$ decreases very rapidly with distance from the mouth of the cavity (like $1/|\mathbf{y}|^3$), and this permits the spanwise integration to be confined to the width $-b/2 < y_3 < b/2$ of the mouth. By similarly neglecting small 'end corrections' at $y_3 \sim \pm b/2$ compared to the contribution to sound generation by the section of the vortex above the mouth in $|y_3| < b/2$, it is also permissible to use a two-dimensional approximation for $\varphi^*(\mathbf{y}) \approx \varphi^*(y_1, y_2)$. This is very convenient, because in two dimensions Laplace's equation $\nabla^2\varphi^* = 0$ can be solved very easily for different positions of the cross-beam using a conventional 'spread sheet' programme on a personal computer [10, 11].

These remarks enable equation (3) for $p_n(\mathbf{x}, t)$ to be rendered in the form

$$p_n(\mathbf{x}, t) = (-1)^n \frac{\rho_o \Gamma U}{|\mathbf{x}|} P\left(t - t_n - \frac{|\mathbf{x}|}{c_o}\right), \quad |\mathbf{x}| \to \infty, \tag{7}$$

where

$$P(t) = -\frac{b}{\pi\mathcal{L}}\frac{U_c}{U}\frac{\partial}{\partial t}\left\{\mathrm{H}(t)\int_0^t \frac{\partial\varphi^*}{\partial y_2}\big(x_r + U_c\lambda, y_c\big)\cos\{\Omega(t-\lambda) + \alpha\}\mathrm{e}^{-\epsilon(t-\lambda)}d\lambda\right\}. \tag{8}$$

By setting $t_n = n\tau_o$, it follows that the overall acoustic pressure $p(\mathbf{x}, t)$ in the far field becomes

$$p(\mathbf{x}, t) = \frac{\rho_o \Gamma U}{|\mathbf{x}|}\sum_{n=-\infty}^{\infty}(-1)^n P\left(t - n\tau_o - \frac{|\mathbf{x}|}{c_o}\right). \tag{9}$$

2.2 The acoustic pressure frequency spectrum

The acoustic pressure $p(\mathbf{x},t)$ given by equation (9) is periodic with fundamental frequency $f_o = 1/2\tau_o$. The pressure spectrum is therefore discrete, and can be expressed in terms of the Fourier transform $\hat{P}(\omega)$ of $P(t)$ defined by

$$\hat{P}(\omega) = \frac{1}{2\pi}\int_{-\infty}^{\infty} P(t)\mathrm{e}^{i\omega t}dt. \tag{10}$$

To do this we first write equation (9) in the form

$$p(\mathbf{x},t) = \frac{\rho_o \Gamma U}{|\mathbf{x}|}\int_{-\infty}^{\infty}\hat{P}(\omega)\left(\sum_{n=-\infty}^{\infty}(-1)^n \mathrm{e}^{i\omega n\tau_o}\right)\mathrm{e}^{-i\omega\left(t-\frac{|\mathbf{x}|}{c_o}\right)}\,d\omega, \tag{11}$$

and introduce the formula [12]

$$\sum_{n=-\infty}^{\infty}(-1)^n \mathrm{e}^{i\omega n\tau_o} = \frac{2\pi}{\tau_o}\sum_{n=-\infty}^{\infty}\delta\left(\omega - \frac{(2n+1)\pi}{\tau_o}\right). \tag{12}$$

The mean square acoustic pressure $\langle p^2(\mathbf{x},t)\rangle$, obtained by averaging over the period $2\tau_o$, is then found to be given by

$$\langle p^2\rangle = 8\left(\frac{\rho_o\Gamma U}{|\mathbf{x}|}\right)^2\omega_o^2\sum_{n=0}^{\infty}\left|\hat{P}\big((2n+1)\omega_o\big)\right|^2, \quad \text{where } \omega_o \equiv 2\pi f_o = \frac{\pi}{\tau_o}, \tag{13}$$

and this defines the frequency spectrum of the sound at resonance.

3. NUMERICAL RESULTS

3.1 Configuration of the cavity and cross-beam

Consider first the case of a cavity and beam for which

$$\frac{b}{L} = 1, \quad \frac{d}{L} = 1, \quad \frac{\ell}{L} = 0.2. \tag{14}$$

For these conditions the real and imaginary parts of the complex resonance frequency $\Omega - i\epsilon$ for the lowest order cavity depth mode are given in columns 2 and 3 of the first row of Table 1. We shall assume that the frequency $f_o \equiv \omega_o/2\pi$ of the periodic vortex shedding from the beam satisfies $f_o\ell/U = 0.2$. At 'lock-on' $\Omega \approx \omega_o$, which occurs when the mean flow Mach number $M = U/c_o$ is given by

$$M = \frac{\Omega L/c_o}{\left(\frac{\Omega}{\omega_o}\right)\left(\frac{\omega_o \ell}{U}\right)\left(\frac{L}{\ell}\right)} \quad \text{at} \quad \Omega \approx \omega_o, \tag{15}$$

i.e. at $M \approx 0.17$. Table 1 lists this value and also (from [4]) the relevant value of the function $\mathcal{F}'(\omega L/2c_o)$ that occurs in the definition (6) of $\mathcal{L}e^{i\alpha}$. The second row of Table 1 gives corresponding values when the depth of the cavity is doubled, but the other dimensions are unchanged.

d/L	$\Omega L/c_o$	$\epsilon L/c_o$	M	$\mathcal{F}'$
1.0	1.098	0.112	0.17	$0.715+i0.665$
2.0	0.64	0.025	0.10	$0.861+i0.398$

Table 1. Resonance conditions for the lowest order depth mode when $b/L = 1$.

We shall calculate the cavity mode radiation at lock-on for five positions of the cross-beam $(x_c,\ y_c)$, labelled Case I - Case V in Table 2

Case	x_c/L	x_r/L	y_c/L
I	-0.8125	-0.7125	
II	-0.5	-0.4	
III	0.0	0.1	0.2125
IV	0.5	0.6	
V	0.8125	0.9125	

Table 2. Positions of the cross-beam.

3.2 Predictions for $d/L = 1$

The cavity mode sound produced by a single vortex is represented by equations (7) and (8). The function $\varphi^*(x_1, x_2)$ in equation (8) has been calculated numerically for the different positions of the cross-beam. Figure 4 depicts the variations of the derivative $\partial\varphi^*/\partial x_2$ (which occurs in the integral on the right of (8)) along the vortex trajectories to the rear of the beam in Cases I - V. Also shown by the broken-line curve is the variation of $\partial\varphi^*/\partial x_2$ when the beam is absent. These results suggest that, apart from its role in generating the vortex, the presence of the beam should not significantly influence the amplitude of the sound produced by the vortex in Cases I, IV and V, i.e. in those cases where the beam is ahead of the leading edge of the cavity, or near or downstream of the trailing edge. The beam produces a significant increase in the potential flow velocity $\partial\varphi^*/\partial x_2$ in Cases II and III (when the beam is near the cavity leading edge and over the central region of the cavity), and it might then be anticipated that cavity mode excitation will be particularly efficient. Evidently the magnitude of this increase depends on the 'blockage' provided by the beam to the reciprocating flow across the mouth of the cavity, a beam of small cross-section would produce proportionately smaller local increases in $\partial\varphi^*/\partial x_2$.

The pressure signature of the sound generated by the release of a single vortex is illustrated by the 'one vortex pressure' curve in Figure 5 (plotted against the nondimensional retarded time $U[t]/L$) for Case III, where the beam spans the centre of the cavity. This has been calculated by setting $n = 0$ in equations (7) and (8), and by taking the vortex convection velocity $U_c = 0.7U$ [1]. The sound exhibits the dominant frequency $\sim \Omega$ of the cavity mode, and decays after about four cycles because of radiation damping. Periodic forcing of the cavity at lock-on by the shedding of successive vortices produces the sustained periodic pressure signature also shown in the figure, and calculated from equation (9) of Section 2. The amplitude of this wave is about four times the maximum for an isolated vortex; moreover it exhibits discontinuities at the retarded times at which vortices are released from the beam, at which times the beam experiences a discontinuous jump in lift and drag [1, 4].

The overall acoustic pressure frequency spectrum is given by (13). The function $|\hat{P}((2n+1)\omega_o)|^2$ is negligible except at its fundamental $n = 0$. The lower series of points • (labelled $d/L = 1$) in Figure 6 represent the variation of this peak or, equivalently, of the sound pressure level

$$10 \times \log_{10}\left(\frac{\langle p^2\rangle}{(\rho_o \Gamma U/|\mathbf{x}|)^2}\right) \quad \text{(dB)} \tag{16}$$

for Cases I - V. These results confirm that the region of high efficiency of cavity mode excitation occurs when the beam is situated above the forward half of the cavity. The broken line interpolation curve indicates the efficiency for other positions of the cross-beam.

3.3 Deep cavity: $d/L = 2$

The calculations have been repeated for a 'deep' cavity, where the depth d is twice the cavity length L, with resonance properties described by the second data row of Table 1. The corresponding sound pressure levels (16) are displayed in Figure 6 (•, upper curve) and are seen to be roughly 5 dB higher than for $d/L = 1$. The efficiency of sound production increases with increasing cavity depth. According to Table 1, the radiation damping (determined by ϵ) is much reduced for the deeper cavity; the resonant oscillations in the mouth of the cavity (i.e. the monopole source strength) can therefore grow to a larger relative amplitude.

4. CONTINUOUS VORTEX SHEDDING

The overall pressure signature in Figure 5 exhibits a discontinuity every half cycle when a vortex is released from the beam. This behaviour is not, perhaps, unexpected, but in practice the relative magnitude of the discontinuities might be smaller because vortex lumps of one sign tend to be shed more smoothly over a finite time interval. These predictions for discrete vortex shedding may be compared with predictions in the opposite extreme in which vorticity is released continuously at frequency ω_o ($\approx \Omega$). In this case the vorticity distribution in the wake (which replaces the succession of discrete vortices $\boldsymbol{\omega}_n$ defined in (2)) can be taken in the form

$$\boldsymbol{\omega} = \frac{\Gamma\omega_o \mathbf{k}}{2U_c} \sin\left(\frac{\omega_o}{U_c}(x_1 - x_r) - \omega_o t\right) \delta(x_2 - y_c), \tag{17}$$

in which case vorticity of total circulation $\pm\Gamma$ is shed from the beam during each half-cycle in which the sine in (17) is $\gtrless 0$.

Equations (1) and (4) may then be used to show that the monopole response of the cavity in the acoustic far field is represented by the pressure distribution

$$\begin{aligned} p(\mathbf{x},t) \;\approx\; & \left(\frac{\rho_o \Gamma U}{|\mathbf{x}|}\right)\left(\frac{b\omega_o^2}{2\pi\mathcal{L}U}\right) \iint_0^\infty \cos\left[\omega_o\left(\frac{y}{U_c} + \tau - [t]\right)\right] \\ & \times \cos(\Omega\tau + \alpha) \mathrm{e}^{-\epsilon\tau} \frac{\partial\varphi^*}{\partial y_2}(x_r + y, y_c)\, dy d\tau, \end{aligned} \tag{18}$$

where $[t] = t - |\mathbf{x}|/c_o$ is the retarded time.

The integration with respect to τ can be performed analytically. By setting $\omega_o = \Omega$ at lock-on, we then easily deduce that (provided $\epsilon \ll \Omega$)

$$p(\mathbf{x},t) \approx \left(\frac{\rho_o \Gamma U}{|\mathbf{x}|}\right)\left(\frac{b\Omega^2}{4\pi\epsilon U\mathcal{L}}\right) \int_0^\infty \frac{\partial\varphi^*}{\partial y_2}(x_r + y, y_c) \cos\left[\Omega\left(\frac{y}{U_c} - [t]\right) - \alpha\right] dy. \tag{19}$$

This is a time-harmonic acoustic pressure at frequency Ω with no overtones. The dotted curve in Figure 5 is the non-dimensional pressure $p(\mathbf{x},t)/(\rho_o\Gamma U/|\mathbf{x}|)$ determined by (19) for Case III of Table 2 when $d/L = 1$. It is the continuous vortex shedding analogue of the solid, discontinuous overall pressure plotted in the same figure and produced by the periodic shedding of discrete vortices.

The predicted overall acoustic wave amplitudes in Figure 5 are practically the same for the two extreme models of discrete and continuous vortex shedding from the cross-beam. This approximate correspondence is also evident from an evaluation of the sound pressure

level (16); the results for continuous shedding are plotted as the open circles in Figure 6 for $d/L = 1,\ 2$. The sound pressure level for continuous shedding is uniformly about 2 - 3 dB below that predicted for discrete vortices for all positions of the beam.

CONCLUSION

Tonal acoustic radiation produced by nominally steady flow past a shallow, rectangular wall cavity is often amplified by the presence of a cross-beam in the flow adjacent to the cavity. At lock-on the frequency of vortex shedding from the beam is equal to one of the resonant frequencies of the cavity. With the exception of cases where the diameter ℓ of the beam is very much smaller than the cavity length L, the efficiency of coupling between the beam and the cavity depends on the position of the beam relative to the cavity opening. The results of this chapter (for $\ell/L = 0.2$) indicate that the coupling is strongest when the beam lies in the forward half of the opening, towards the cavity leading edge. This conclusion is based on predictions of the radiation for two alternative and extreme models of vortex shedding from the beam (periodically shed discrete vortices and continuously shed time-harmonic vorticity); it also appears to be independent of cavity depth provided the mean flow Mach number is small at lock-on (say less than about 0.2).

It should be remarked, that at lock-on the motion of the mean shear layer spanning the mouth of the cavity must include components oscillating at the same frequency as the vortex shedding from the beam. The contribution of the sound generated by this motion is not included in our analysis; it arises principally from the interaction of shear layer vorticity with the downstream region of the cavity [1, 3], which could well be enhanced when the beam is near or downstream of the cavity trailing edge. Also, the overall amplitude of the sound at lock-on depends on the magnitude of the circulation Γ of the shed vorticity. At low Mach numbers this is likely to be controlled by nonlinear mechanisms that are not influenced significantly by the compressibility of the flow, although there may be some dependence on the location of the cross-beam. This dependence on beam position and the possible couplings with the mean shear layer will need to be determined by experiment or by large scale numerical simulations of the kind described recently by Mallick *et al.* [5].

REFERENCES

1. M. S. Howe 1998 *Acoustics of fluid-structure interactions*, Cambridge University Press.
2. M. S. Howe 1997 Edge, cavity and aperture tones at very low Mach numbers. *Journal of Fluid Mechanics* **330**, 61 - 84.
3. M. S. Howe 2002 Mechanism of sound generation by low Mach number flow over a wall cavity. Chapter 1 and *Journal of Sound and Vibration* (in press).
4. M. S. Howe 2003 Wall-cavity acoustic Green's function at low Mach number. Chapter 2 and *International Journal of Aeroacoustics* **2**, 347 - 365.
5. S. Mallick, R. Shock and V. Yakhot 2003 Numerical simulation of the excitation of a Helmholtz resonator by a grazing flow. *Journal of the Acoustical Society of America* **114**, 1833 - 1840.
6. D. Rockwell and E. Naudascher 1978 Review - self-sustaining oscillation of flow past cavities. *Transactions of the American Society of Mechanical Engineers, Journal of Fluids Engineering* **100**, 152 - 165.
7. D. Rockwell 1983 Oscillations of impinging shear layers. *American Institute of Aeronautics and Astronautics Journal* **21**, 645 - 664.
8. R. D. Blevins, R. D. 1984 Review of sound induced by vortex shedding from cylinders. *Journal of Sound and Vibration* **92**, 455 - 470.
9. R. D. Blevins 1985 The effect of sound on vortex shedding from cylinders. *Journal of Fluid Mechanics* **161**, 217 - 237.
10. Morishita, E. 1999 Spreadsheet fluid dynamics. *Journal of Aircraft* **36**, 720 - 723.
11. A. Winslow and M. S. Howe 2003 Stepwise approximation of an optimally flared tunnel portal. *Journal of Sound and Vibration* (in press).
12. M. J. Lighthill 1958 *An introduction to Fourier analysis and generalised functions.* Cambridge University Press.

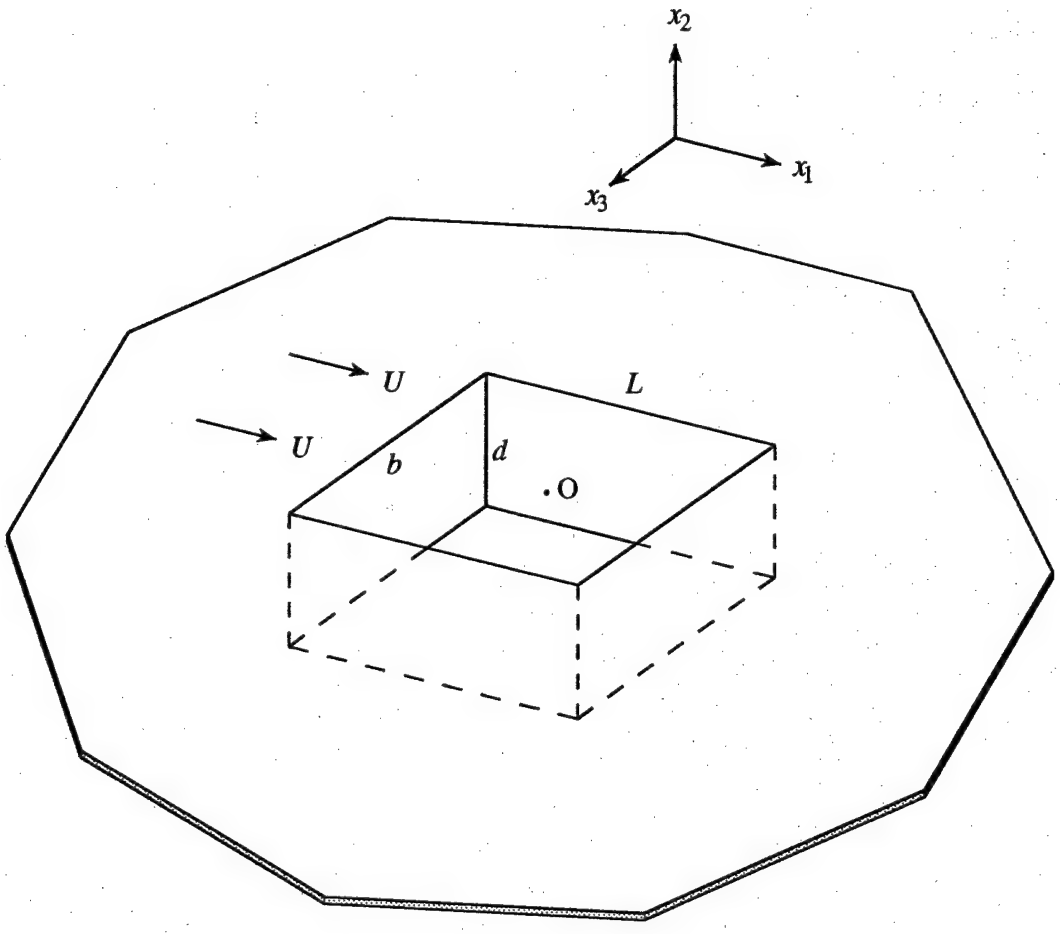

Figure 1. Rectangular wall cavity of depth d and streamwise length L in the presence of low Mach number steady flow at speed U in the x_1-direction.

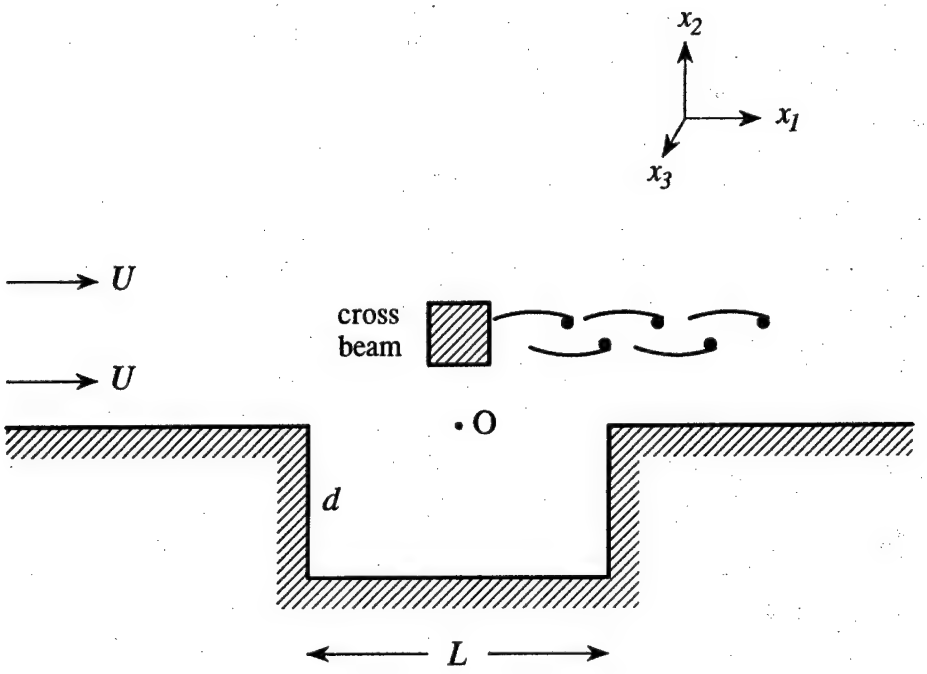

Figure 2. Vortex shedding from a square-sectioned cross-beam adjacent to the cavity.

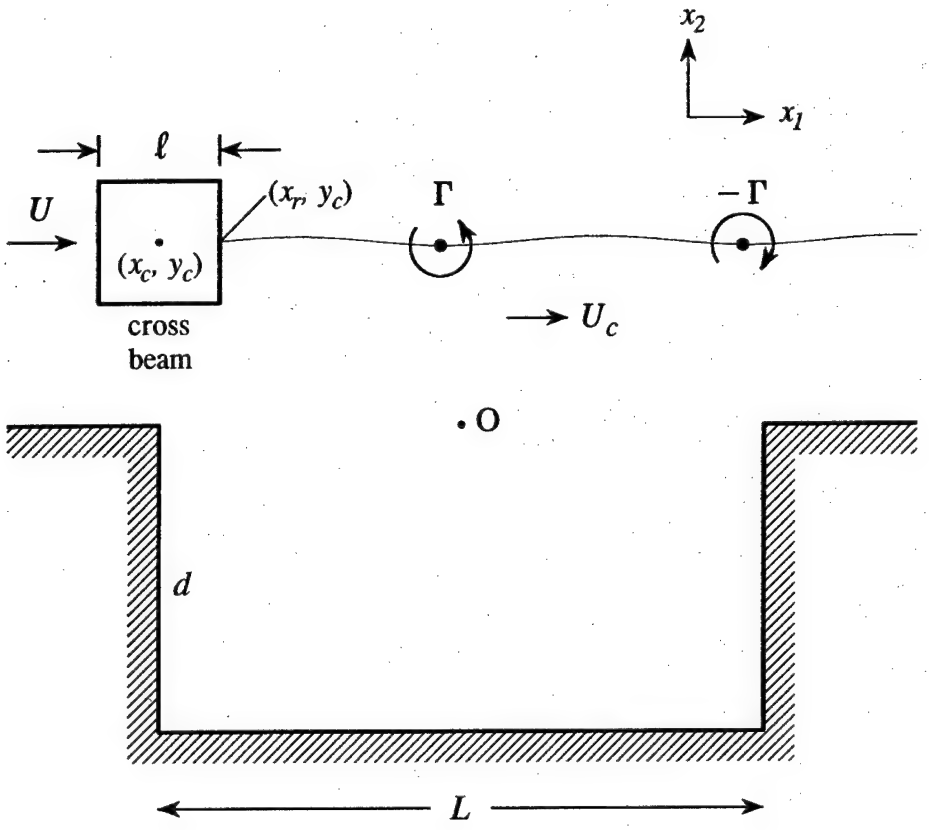

Figure 3. Simplified model of periodic vortex shedding from a square-sectioned beam whose axis lies along $x_1 = x_c$, $x_2 = y_c$. The beam is shown positioned for Case II of Section 3.

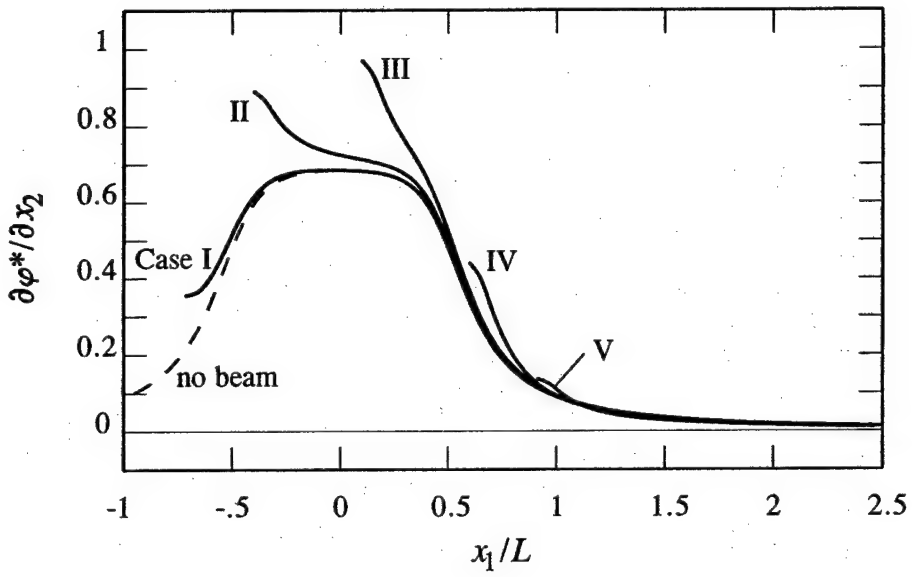

Figure 4. Variation of $\partial\varphi^*/\partial x_2$ along the trajectory of a shed vortex for cases I - V of Table 1 (——), and along the nominal trajectory of a vortex in the absence of the cross-beam (– – –).

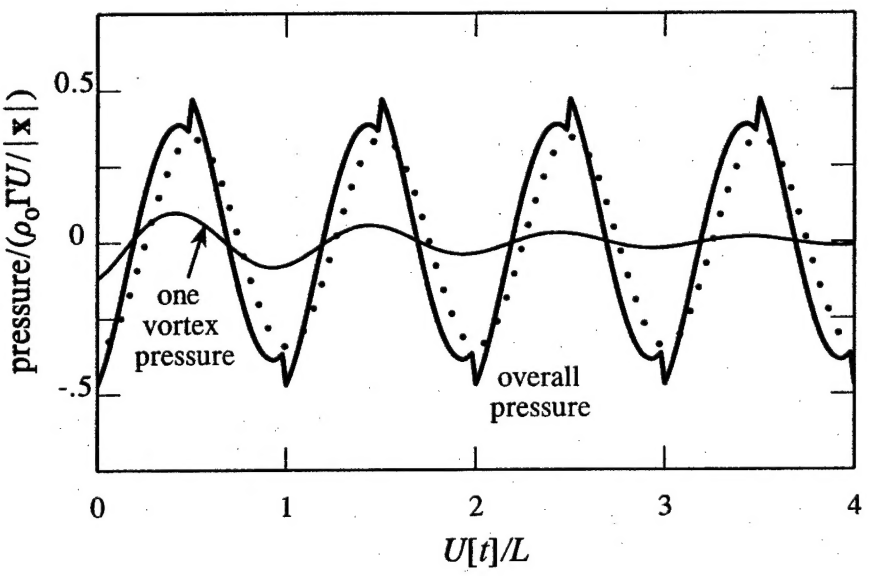

Figure 5. Predicted acoustic pressures when the cross-beam is directly above the cavity (Case III of Table 2) and $d/L = 1$: ——, overall pressure signature of the lowest order cavity mode radiation when the wake consists of a sequence of discrete, rectilinear vortices; ——, the exponentially damped cavity mode radiated pressure produced by one vortex; ·····, the overall pressure signature for the continuous vortex wake of Section 4.

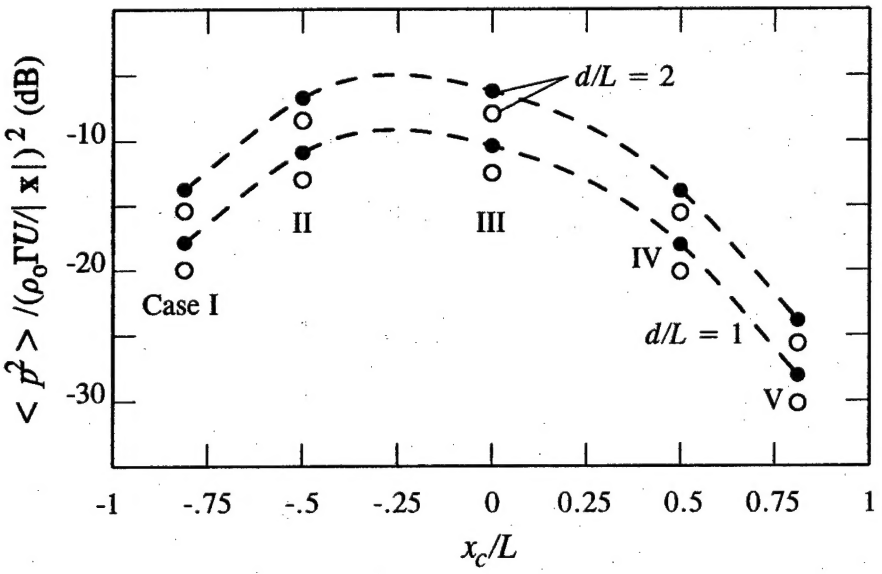

Figure 6. Predicted dependence of the sound pressure level $10 \times \log_{10}\left(\langle p^2 \rangle / (\rho_o \Gamma U/|\mathbf{x}|)^2\right)$ on the streamwise position of the cross-beam for $d/L = 1,\ 2$ when the wake of the cross-beam is modelled by discrete, rectilinear vortices (• • •). The open circles are the corresponding predictions for the continuous, vortex sheet wake of Section 4.

DISTRIBUTION

Dr. L. Patrick Purtell — 1 copy
Office of Naval Research
Code 333
800 North Quincy Street
Arlington, VA 22217-5660

Defense Technical Information Center — 1 copy
8725 John J. Kingman Road, Ste 0944
Fort Belvoir, VA 22060-5320

Naval Research Laboratory — 1 copy
Code 5227
4555 Overlook Avenue SW
Washington DC 20375-5320

Dr. W. K. Blake — 1 copy
Carderock Division,
Naval Surface Warfare Center (Code 7051)
9500 MacArthur Boulevard
West Bethesda, MD 20817-5700.

Dr. T. M. Farabee — 1 copy
Carderock Division,
Naval Surface Weapons Center (Code 725)
9500 MacArthur Boulevard
West Bethesda, MD 20817-5700.

Dr. G. C. Lauchle — 1 copy
Applied Research Laboratory
PO Box 30
State College, PA 16804.

REPORT DOCUMENTATION PAGE

Form Approved
OMB No. 0704-0188

1. REPORT DATE	2. REPORT TYPE	3. DATES COVERED *(From - To)*
03-01-2004	Final	03-07-2002 to 30-11-2003

4. TITLE AND SUBTITLE

Wall-cavity aeroacoustics at low Mach number

5a. CONTRACT NUMBER

5b. GRANT NUMBER
N00014-02-1-0549

5c. PROGRAM ELEMENT NUMBER

6. AUTHOR(S)

Michael S. Howe

5d. PROJECT NUMBER

5e. TASK NUMBER

5f. WORK UNIT NUMBER

7. PERFORMING ORGANIZATION NAME(S) AND ADDRESS(ES)

Boston University
College of Engineering
110 Cummington Street
Boston MA 02215

8. PERFORMING ORGANIZATION REPORT NUMBER

AM-04-001

9. SPONSORING / MONITORING AGENCY NAME(S) AND ADDRESS(ES)

Office of Naval Research Dr. L. Patrick Purtell
Code 333

10. SPONSOR/MONITOR'S ACRONYM(S)

11. SPONSOR/MONITOR'S REPORT NUMBER(S)

12. DISTRIBUTION / AVAILABILITY STATEMENT

Approved for Public Release; Distribution Unlimited

13. SUPPLEMENTARY NOTES

14. ABSTRACT

Theoretical and numerical analyses are made of the mechanism of sound production by nominally steady low Mach number flow over a rigid shallow wall cavity. At very low Mach numbers the dominant source of sound is the unsteady drag, and the aeroacoustic dipole source accompanying this force. A monopole source dependent on the compression of fluid within the cavity is smaller by a factor of the order of the flow Mach number M. However, numerical simulations for M as small as 0.1 have predicted significant radiation in directions normal to the wall. This anomaly is investigated by using an acoustic Green's function tailored to cavity geometry. The Green's function is extended to examine the production of sound by vortex shedding at 'lock-on' from a cross-beam adjacent

15. SUBJECT TERMS

Aerodynamic sound, wall cavity, vortex sound, lock-on, cavity mode, cross-beam

16. SECURITY CLASSIFICATION OF:			17. LIMITATION OF ABSTRACT	18. NUMBER OF PAGES	19a. NAME OF RESPONSIBLE PERSON
a. REPORT Uncl	b. ABSTRACT Unclassified	c. THIS PAGE Unclassified		81+ii	19b. TELEPHONE NUMBER *(include area code)*